Knickpoints and crescentic bedform interactions in submarine channels

Chen, Ye; Parsons, Daniel R.; Simmons, Stephen M.; Williams, Rebecca; Cartigny, Matthieu J.B.; Hughes Clarke, John E.; Stacey, Cooper D.; Hage, Sophie; Azpiroz-Zabala, Maria; More Authors

DOI
10.1111/sed.12886

Publication date
2021

Document Version
Accepted author manuscript

Published in
Sedimentology

Citation (APA)
Chen, Y., Parsons, D. R., Simmons, S. M., Williams, R., Cartigny, M. J. B., Hughes Clarke, J. E., Stacey, C. D., Hage, S., Azpiroz-Zabala, M., & More Authors (2021). Knickpoints and crescentic bedform interactions in submarine channels. *Sedimentology*, *68*(4), 1358-1377. https://doi.org/10.1111/sed.12886

Knickpoints and crescentic bedform interactions in submarine channels

Ye Chen[1,2], Daniel R. Parsons[1], Stephen M. Simmons[1], Rebecca Williams[2], Matthieu J.B. Cartigny[3], John E. Hughes Clarke[4], Cooper D. Stacey[5], Sophie Hage[6,7], Peter J. Talling[3], Maria Azpiroz-Zabala[6,8], Michael A. Clare[6], Jamie L. Hizzett[6,9], Maarten S. Heijnen[6,9], James E. Hunt[6], D. Gwyn Lintern[5], Esther J. Sumner[9], Age J. Vellinga[6,9], Daniela Vendettuoli[6,9]

Email: Ye.Chen-2016@hull.ac.uk

This is a post-peer-review, pre-copyedit version of an article published in Sedimentology. The final authenticated version is available online at: https://doi.org/10.1111/sed.12886.

Knickpoints and crescentic bedform interactions in submarine channels

Ye Chen[1,2], Daniel R. Parsons[1], Stephen M. Simmons[1], Rebecca Williams[2], Matthieu J.B. Cartigny[3], John E. Hughes Clarke[4], Cooper D. Stacey[5], Sophie Hage[6,7], Peter J. Talling[3], Maria Azpiroz-Zabala[6,8], Michael A. Clare[6], Jamie L. Hizzett[6,9], Maarten S. Heijnen[6,9], James E. Hunt[6], D. Gwyn Lintern[5], Esther J. Sumner[9], Age J. Vellinga[6,9], Daniela Vendettuoli[6,9]

[1]Energy and Environment Institute, University of Hull, Hull, HU6 7RX, UK

[2]Department of Geography, Geology and Environment, University of Hull, Hull, HU6 7RX, UK

[3]Departments of Earth Sciences and Geography, University of Durham, Stockton Road, Durham, DH1 3LE, UK

[4]Center for Coastal and Ocean Mapping, University of New Hampshire, Durham, New Hampshire 03824, USA

[5]Natural Resource Canada, Geological Survey of Canada, Sidney, British Columbia V8L 4B2, Canada

[6]Ocean Biogeoscience, National Oceanography Centre, Southampton SO14 3ZH, UK

[7]Department of Geoscience, University of Calgary, Calgary, T2N 1N4 AB, Canada

[8]Faculty of Civil Engineering and Geosciences, Delft University of Technology, Delft, The Netherlands

[9]School of Ocean and Earth Sciences, University of Southampton, Southampton SO14 3ZH, UK

Associate Editor – Arnoud Slootman

Short Title – Knickpoints and crescentic bedform interactions

ABSTRACT

Submarine channels deliver globally important volumes of sediments, nutrients, contaminants and organic carbon into the deep sea. Knickpoints are significant topographic features found within numerous submarine channels, which most likely play an important role in channel evolution and the behaviour of the submarine sediment-laden flows (turbidity currents) that traverse them. Although prior research has linked supercritical turbidity currents to the formation of both knickpoints and smaller crescentic bedforms, the relationship between flows and the dynamics of these seafloor features remains poorly constrained at field-scale. This study investigates the distribution, variation and interaction of knickpoints and crescentic bedforms along the 44 km long submarine channel system in Bute Inlet, British Columbia. Wavelet analyses on a series of repeated bathymetric surveys reveal that the floor of the submarine channel is composed of a series of knickpoints that have superimposed, higher-frequency, crescentic bedforms. Individual knickpoints are separated by hundreds to thousands of metres, with the smaller superimposed crescentic bedforms varying in wavelengths from *ca* 16 m to *ca* 128 m through the channel system. Knickpoint migration is driven by the passage of frequent turbidity currents, and acts to redistribute and reorganize the crescentic bedforms. Direct measurements of turbidity currents indicate the seafloor reorganization caused by knickpoint migration can modify the flow field and, in turn, control the location and morphometry of crescentic bedforms. A transect of sediment cores obtained across one of the knickpoints show sand–mud laminations of deposits with higher aggradation rates in regions just downstream of the knickpoint. The interactions between flows, knickpoints and bedforms that are documented here are important because they likely dominate the character of preserved submarine channel-bed deposits.

Keywords: Crescentic bedforms; Knickpoints; Sedimentary records; Submarine channels; Turbidity currents

INTRODUCTION

Submarine channels are conduits for turbidity currents, which are one of the most volumetrically important processes for the delivery of sediments, nutrients, organic carbon and pollutants into the deep sea (Bouma, 2000; Peakall *et al.*, 2007; Paull *et al.*, 2010; Azpiroz-Zabala *et al.*, 2017). Turbidity currents are not only important for global sediment transport (Peakall & Sumner, 2015), but also because of the hazards they pose to seafloor infrastructure, such as communication cables or pipelines (Piper *et al.*, 1999; Cooper *et al.*, 2013; Carter *et al.*, 2014). The triggers that generate such powerful flows have been ascribed to submarine landslides (Prior *et al.*, 1981; Obelcz *et al.*, 2017), plunging of hyperpycnal river discharge (Mulder *et al.*, 2003; Dietrich *et al.*, 2016), sediment remobilized by internal waves and tides (Puig *et al.*, 2004; Pomar *et al.*, 2012; Normandeau *et al.*, 2014) and sediment settling from surface river plumes (Parsons *et al.*, 2001; Hizzett *et al.*, 2017; Hage *et al.*, 2019).

Current understanding of how these currents transport sediments mainly derives from interpreting their deposits (turbidites) in the field, together with laboratory scale (flume) experiments and numerical modelling (e.g. Kuenen & Migliorini, 1950; Bennett & Best, 1995; Best, 2005b; Talling *et al.*, 2012; Cartigny *et al.*, 2014; Kostic, 2014; Hage *et al.*, 2018). These methods have produced major advances in understanding, but until recently there were very few direct measurements from turbidity currents in action (Inman *et al.*, 1976; Prior *et al.*, 1987; Talling *et al.*, 2015; Clare *et al.*, 2016). New detailed insights have been gained through direct monitoring of active turbidity currents, in particular using acoustic Doppler current profilers (ADCP) (e.g. Hughes Clarke, 2016; Paull *et al.*, 2018; Simmons *et al.*, 2020). These achievements provide

extraordinary new insights into the flow fields and the internal structure and behaviour of turbidity currents (Khripounoff *et al.*, 2009; Talling *et al.*, 2013; Xu *et al.*, 2014; Hughes Clarke, 2016; Azpiroz-Zabala *et al.*, 2017), their interaction with the seafloor and their resultant sedimentary deposits (e.g. Smith *et al.*, 2007; Paull *et al.*, 2018; Vendettuoli *et al.*, 2019; Guiastrennec-Faugas *et al.*, 2020; Heijnen *et al.*, 2020).

Prior studies have recognized the prevalence of crescentic bedforms over a range of subaqueous depositional settings, including delta slopes (Hughes Clarke *et al.*, 2012; Turmel *et al.*, 2015; Hage *et al.*, 2018), the axis of shallow-water submarine channels (Smith *et al.*, 2005; Hughes Clarke *et al.*, 2014; Normandeau *et al.*, 2014; 2015), the axis of deep-water channels (Babonneau *et al.*, 2013; Heijnen *et al.*, 2020) and across unconfined submarine fans (Normark *et al.*, 2002; Shao *et al.*, 2021). Recent bathymetric mapping has revealed that the upper sections of submarine channels are often dominated by upslope-migrating crescentic bedforms (Symons *et al.*, 2016; Hughes Clarke, 2016). Integration of sediment cores with repeat seafloor bathymetric surveys showed how frequent, supercritical turbidity currents can drive the upstream-migration of crescentic bedforms, reworking and reorganizing previous deposits (Hage *et al.*, 2018; Vendettuoli *et al.*, 2019). This reworking was found to leave behind ungraded or poorly-graded units of massive sands that infill scours (Hage *et al.*, 2018; Vendettuoli *et al.*, 2019; Englert *et al.*, 2020). These bedforms also shed light on the transition from river flow to submarine density flows and on the resulting modifications of seafloor geomorphology, and can be linked to observations of back-stepping beds and scour fills preserved in the sedimentary record (Hage *et al.*, 2018).

Another important morphological feature found in a number of submarine channels are knickpoints, which comprise abrupt changes in channel gradient and can vary in morphology along the channel (Mitchell, 2006; Paull *et al.*, 2010; Heijnen *et al.*, 2020).

Herein, knickpoints are defined as steep steps on the order of tens to hundreds of metres in height, differentiated from smaller crescentic bedforms by the larger scales and sharper crests (see Heijnen *et al.*, 2020). This definition of knickpoint or crescent bedform is based on a description of morphological features. Those definitions do not imply specific flow types or processes (for example, subcritical or supercritical flow) as diagnosed in some previous studies, where large-scale 'cyclic step' morphologies are referred to as supercritical flow derived knickpoints (e.g. Postma & Cartigny, 2014; Zhong *et al.*, 2015). Knickpoints in rivers are known to play a major role in governing subaerial channel formation, evolution and adjustment in response to either regional or local perturbations in fluvial/alluvial systems (Gilbert, 1895; Holland, 1974; Hayakawa & Matsukura, 2003; Cantelli & Muto, 2014; Pederson & Tressler, 2012; Baynes *et al.*, 2018). However, similar features in submarine environments are much less well understood. First-order questions remain concerning how submarine knickpoints migrate upstream, and how knickpoint migration interacts with smaller-scale associated crescentic bedforms, influencing the longer-term submarine channel evolution and the resulting sedimentary record. Although the morphology and formation mechanisms might differ, knickpoints are observed globally in various settings, and have been reported from erosional submarine canyons (for example, San Antonia Canyon, offshore Chile; Mitchell, 2006), open continental slopes (New Jersey continental slope; Mitchell, 2006), deep-water 'waterfalls' (Monterey Fan; Masson *et al.*, 1995), headless channels (Girardclos *et al.*, 2012) and submarine channel meander bend cut-offs (Cantelli & Muto, 2014; Sylvester & Covault, 2016). In a previous study of Bute Inlet, Heijnen *et al.* (2020) showed that submarine knickpoints can dominate submarine channel and channel-bend evolution, and can migrate upstream very rapidly (hundreds of metres per year). However, the influence and

interactions of knickpoints and their migration with superimposed crescentic bedforms, and the associated sedimentary signature that results, remain poorly documented. Here a sequence of bathymetric surveys acquired in Bute Inlet, British Columbia, Canada (see Heijnen *et al.*, 2020, for more details) are analysed. The first aim is to investigate the variability in seafloor morphology across a range of scales along the length of the system. The second aim is to explore the details of knickpoint migration, and the relationships between knickpoint dynamics and the response of superimposed crescentic bedforms. The third aim is to investigate the depositional architecture and sedimentary facies over a single closely-studied knickpoint through a suite of sediment cores, which in turn sheds light on the impact of spatial and temporal morphological changes and the interactions with turbidity current dynamics. A new knickpoint model is proposed that captures the coupling between turbidity currents, knickpoints and superimposed crescentic bedforms, and their potential impact on longer-term channel morphological evolution and preserved channel-floor deposits.

STUDY SITE

Bute Inlet is located along the coast of British Columbia, Canada (Fig. 1). The glacially carved fjord has a length of over 70 km. It hosts an active submarine channel that is 44 km long, developing under the activity of traversing turbidity currents (Bornhold *et al.*, 1994; Conway et al., 2012; Heijnen *et al.*, 2020). The channel extends to a water depth of 600 m at the distal end of the system, where it terminates in a depositional lobe. Two main rivers, the Homathko and Southgate rivers, drain large watersheds within the mountainous hinterlands, and feed into Bute Inlet at the head of the fjord, contributing respectively *ca* 80% and *ca* 15% to the total river discharge (Fig. 1; Syvitski & Farrow, 1983). The remaining 5% is provided by minor tributaries of the fjord

(Syvitski & Farrow, 1983; Heijnen *et al.*, 2020). Discharge into Bute Inlet is highly seasonal, peaking in July because of snow and ice melt from the interior watershed. Short-lived flood discharges can be up to 1000 m^3/s during peak season in the summer and early autumn (Bornhold *et al.*, 1994; Canadian Hydrographic Office data available from https://wateroffice.ec.gc.ca/). The lowest input occurs in the winter months as the precipitation is stored as snow and ice at higher altitudes in the watershed. With a range of 4 to 5 m during spring tides, the fjord is also affected by a relatively strong tidal forcing (Hughes Clarke, 2016). Very fine to coarse sand or fine gravel dominate the fjord delta top and the adjoining submarine channel (Syvitski & Farrow, 1983; Zeng *et al.*, 1991). A series of knickpoints has been discovered along the submarine channel of Bute Inlet, and has been described in detail previously (Gales *et al.*, 2019; Heijnen *et al.*, 2020).

METHODS AND MATERIALS

Bathymetry

Repeat multibeam bathymetric survey data was acquired from Bute Inlet over a period from 2008 to 2018 (for more details see Heijnen *et al.*, 2020). The bathymetric data cover the entire submarine-channel system, and they were obtained using a Kongsberg Maritime EM710 Multibeam Echosounder system (Kongsberg Gruppen ASA, Kongsberg, Norway) operating at 70–100 kHz, deployed on the Canadian Coastguard Research vessel *CCGS Vector*. These data were supplemented with higher-resolution bathymetric data from October 2016 and November 2018 surveys at the two fjord-head river deltas (i.e. Homathko River Delta and Southgate River Delta), which are used for the detailed analysis of crescentic bedform characteristics in the *Crescentic bedform characteristics at the Homathko and Southgate deltas* section

(see supplementary data Table 1). These complementary data were acquired using a Reson Seabat 7125 Multibeam Echo Sounder (Teledyne Reson AS, Slangerup, Denmark) mounted over the side of University of Victoria's *R/V Strickland*. This Multibeam Echo Sounder system operates at a frequency of either 200 or 400 kHz and has centimetric precision, with a horizontal resolution of tens of centimetres (Parsons *et al.*, 2005; Leyland *et al.*, 2016). All bathymetric data were processed using CARIS-HIPS software, applying sound velocity corrections, and pitch-roll-yaw calibrations. The accuracy of vessel position was improved post-survey using POSPac software which uses combined positional data fixes from local GPS stations recorded during the survey period. These positions were imported into CARIS within the processing workflow. CARIS was used to generate integrated bathymetric surfaces that were then exported to ArcGIS to analyse the bed elevation data, extract channel longitudinal profiles, and generate difference maps.

Turbidity current dynamics

Six down-looking acoustic Doppler current profilers (ADCP) were deployed on moorings along the submarine channel for a duration of about four months from June to October 2016. These moorings were labelled ADCP6 to ADCP1, moving from the proximal delta to the distal lobe (Fig. 1). These moored ADCPs were positioned from the proximal, upper section of the channel to the distal lobe, with two ADCPs placed close together (ADCP5 and ADCP4) across a particular knickpoint for closer study, located *ca* 11 km downstream of the fjord-head along the channel course. The ADCPs were suspended above the channel bed via a two-point mooring for the shallower four ADCPs (ADCP6 to ADCP3), and suspended on a syntactic midwater buoy for the two deeper distal moorings (Clare *et al.*, 2020; for more details see supplementary data

Table 2). Acoustic backscatter data were recorded at all moorings, with one ADCP also capturing three-dimensional flow velocity data. The six ADCPs captured the passage and evolution of episodic turbidity currents through their four-month deployment as the flows progressed through the channel system. About 20 turbidity currents were observed during the first six-week period of deployment. The most proximal mooring (ADCP6) stopped recording after a particularly powerful turbidity-current event on 31 July 2016; hence no record was generated at that location for the remaining 2.5 months (Fig. 2). Throughout the monitoring period, most of the flows dissipated in the proximal part of the channel system, with 11 events observed at the primary study knickpoint (located between ADCP5 and ADCP4; Figs 1 and 2). Only three flow events traversed the entire channel reaching its lower section, and approaching the distal lobe zone. Because this study mainly focuses on channel morphological features and sedimentary architectures, detailed analysis of the turbidity current ADCP data is not presented in the *Results* section. Rather, this study uses ADCP data to determine turbidity current timing, frequency and front speeds, and utilises this information to relate knickpoint migration and sediment deposits to turbidity currents.

Wavelet analysis and bedform discrimination

The quantification of bedform geometry is essential to understanding the interactions between flow and bed morphology (Kostaschuk, 2006), explaining cross-strata formation processes (Reesink & Bridge, 2011), and quantifying sediment transport over the bedforms (Wilbers & Ten Beinke, 2003). The bedform geometries were extracted along transect lines at both Homathko and Southgate deltas, and were analysed with the bedform tracking tool (BBT; Van der Mark *et al.*, 2008) in Matlab®, along with manually picking out the bedform features. The differences in bedform

dimensions through time and space were quantified and analysed using analysis of variance (ANOVA) methodologies. Wavelet analysis was also performed on the bedform spatial series, using the Bedform-ATM (Bedform analysis toolkit for multiscale modelling) code (Gutierrez *et al.*, 2013, 2018). First, the longitudinal channel profile was extracted and detrended using a moving average method. The gradient was derived from a fitted trendline and the amplitude was calculated as the residual after subtracting the trendline from the series. A one-dimensional continuous wavelet analysis approach was adopted (Torrence & Compo, 1998) and applied to the detrended along-channel residual of the transects. The wavelet power spectrum demonstrates the dominant constituent wavelengths along the channel as a function of distance. Values that fall outside a cone of influence and that fall below significant power levels, which are limited by the length of the series and/or noise (Gutierrez *et al.*, 2018), are screened out.

Sediment core analysis

Seven box cores and one piston core were collected in this study, covering the study knickpoint and an area farther downstream (Fig. 1A). The piston core (STN007, 170 cm) was collected during the June 2016 survey and the seven box cores were collected during the October 2016 survey. The October to June 2016 bathymetric difference maps show net deposition of between 1 m and 4 m adjacent to these box cores. Given the shorter length of the box cores (up to *ca* 0.32 m), these bathymetric differences represent deposits laid down during the survey period from June to October 2016. Cores were logged at the Institute of Ocean Science, British Columbia, to provide a description of the depositional signatures resulting from the passage of turbidity currents over the knickpoint and the superimposed bedforms. The orientation

of the cores could not be controlled during the sampling meaning that any dip orientations could not be recovered from the cores.

RESULTS

Distribution of knickpoints and crescentic bedforms along a submarine channel

The bathymetric difference map between surveys conducted in 2008 and 2018 is shown in Fig. 1. The difference map highlights the geomorphology of the submarine system and reveals a kilometre-scale pattern of alternating erosion and deposition along the entire channel across the ten years of the survey (see Heijnen *et al.*, 2020, for additional analysis). Two primary zones of erosion are present between the locations of ADCP4 and ADCP3, and between ADCP3 and ADCP2, where multiple knickpoints occur (i.e. termed 'knickpoint zones' in Heijnen *et al.*, 2020). Repeat bathymetric surveys over shorter timescales reveal that these knickpoints have been actively migrating upstream during at least the last ten years, resulting in locally intensive incision and entrenchment (Heijnen *et al.*, 2020). Depositional zones also occur in the relatively flatter sections along the channel slope.

A thalweg-parallel longitudinal profile from the October 2016 survey, with a length of over 44 km, is shown in Fig. 3A. The channel gradient decreases from *ca* 8° at the delta front to <0.25° distally. The vertical black lines in Fig. 3A mark the location of the major knickpoints along the channel with a slope gradient variation from 1.0° to 0.25°. Knickpoint locations correspond to maxima in both channel gradient (Fig. 3B) and bedform amplitude (Fig. 3C), with apparent clustering. The wavelet power spectrum of the detrended profile shows that knickpoint locations correspond to the increases in spectral power of wavelengths, typically in the range of *ca* 16 to *ca* 128 m (Fig. 3D). These wavelengths are typical of the crescentic bedforms visible in bathymetric data.

Crescentic bedforms associated with knickpoints are a pervasive feature of the entire channel system, as shown in Fig. 3C, with the data indicating that bedform characteristic wavelengths decrease downstream of knickpoints.

Knickpoints are typically separated by lower-gradient regions that stretch over distances of hundreds to thousands of metres (Heijnen *et al.*, 2020). Two main knickpoint zones (corresponding to the red erosional zones in Fig.1) are present in the medial (from *ca* 17 km to 22 km) and lower channel sections (from *ca* 30 km to 34 km). There is seemingly no systematic pattern in the scales (amplitude, gradient and wavelength) of knickpoints observed along the entire channel. However, the frequency of crescentic bedforms appears to be higher in the shallower proximal part of the system than the deeper part of the channel (Fig. 3C), although this may be related to the decline in sensing capability with increasing water depth.

Crescentic bedform characteristics at the Homathko and Southgate deltas

The clinoforms of the Homathko and Southgate deltas are dominated by trains of crescentic bedforms, with zones of both degradation and aggradation across a range of incoming riverine flow conditions, as evident from repeat mapping during the study period (Fig. 4). The subaqueous channel morphologies for the Homathko and Southgate deltas are shown in Fig. 4C and 4D, respectively. The Homathko Delta clinoform gradient varies from *ca* 8° to *ca* 3°. A range of flow channel/pathways are observed across the clinoform delta front, notably shallower than *ca* 30 m water depth, where there is an average seabed gradient of 6.25°. At *ca* 75 m water depth these flow pathways merge into three principal channels in the along the slope, and then into a single channel at the base of the delta clinoform, at *ca* 115 m depth. A large subaqueous ridge is present at the south-west side of the delta (Fig. 4A, labelled ‘a’)

with a maximum width of 100 m, height of 30 m above the channel bed and a length of 1030 m (Fig. 4C). The ridge extends from 40 m to 115 m water depth and has been slowly eroded over the ten-year survey period, likely due to flank failures.

At Southgate Delta, the clinoform slope has a steeper gradient compared to Homathko Delta (Fig. 4B). The main channel, to the north of the delta, is dominated by large-scale crescentic bedforms. A few smaller channels are situated in the central section of the delta clinoform. In the southern section of the delta, a narrower shallow channel exists. All these delta clinoform channels merge into one wider conduit at a depth of *ca* 130 m.

Wavelet analysis (Fig. 5) allows the examination of the complex relationship between bedform scales and the underlying channel morphology. Crescentic-bedform wavelengths generally increase as water depth increases and as channel gradient declines down the clinoform (Fig. 5C and F). Despite the different gradient profiles of the two deltas, the ranges of dominant crescentic bedform wavelengths show similar trends down the clinoform face.

A statistical analysis of the handpicked bedform geometric features obtained from higher-resolution bathymetric mapping is given in Fig. 6. Comparisons of bedform height, wavelength and steepness (the ratio of bedform height to wavelength) are shown for the Homathko Delta surveys conducted in both October 2016 and November 2018, and for the Southgate Delta survey of November 2018. The following observations are made:

(1) Crescentic bedform heights mostly vary from 0.5 m to 2.0 m on both delta clinoforms. The mean value of bedform height of the Homathko 2018 survey data is smaller than both the Homathko 2016 and Southgate 2018 survey data. The

Homathko 2018 survey data show a higher proportion of bedform heights below 1 m and a wider variability (Fig. 6A).

(2) The bedform wavelengths of the Homathko 2018 survey vary from 5 m to 40 m. Over two-thirds of the bedform wavelengths fall into the range from 15 m to 45 m in the Homathko 2016 survey data, with a slightly higher percentage of longer wavelengths of over 50 m (Fig. 6B).

(3) As shown in Fig. 6C, over 90% of the steepness values are within the range from 0.01 to 0.09. The Homathko 2018 survey data have dominant steepness values of *ca* 0.06, which are higher than the mean of steepness in both the Homathko 2016 and Southgate 2018 survey data. As such, although the height and wavelength are smaller, the Homathko 2018 survey data tend to show higher bedform steepness values.

Generally, the bedform heights and wavelengths in the October 2016 survey of the Homathko Delta are higher than those determined from the November 2018 survey. Additionally, the differences in steepness are analysed by using the analysis of variance (ANOVA), which shows that the results fall into the 95% significance level, suggesting that there are statistically significant differences of crescentic bedform steepness between both the Homathko 2016 and 2018 data, as well as the Homathko 2018 and Southgate 2018 datasets.

The influence of knickpoints on crescentic bedforms

The morphology of the Bute Inlet submarine channel is dominated by multiple knickpoints that are superimposed by higher-frequency, smaller crescentic bedforms (Fig. 3). Knickpoints migrate upstream through the erosion of the steep knickpoint face (Heijnen *et al.*, 2020). The geometry and scale of the study knickpoint is illustrated in

360 the red dashed box ‘b’ in Fig. 3D and the red dashed box in Fig. 1A. The difference in
361 water depth over the knickpoint is revealed by the repeat seafloor surveys in June
362 2016 and May 2018, and is shown in Figs 7 and 8.

363 Wavelet analysis (Fig. 8) across the study knickpoint indicates a spatial variability in
364 the wavelengths (extending from *ca* 16 to 128 m) of the crescentic bedforms that are
365 superimposed across the larger knickpoint. In the June 2016 survey, crescentic
366 bedforms occur within a region *ca* 140 m downstream of the knickpoint. Further
367 downstream, crescentic bedforms return to much shorter wavelengths, which are
368 similar in scale to bedforms located just upstream of the knickpoint. The wavelet power
369 spectrum from the May 2018 survey shows similar bedform scale patterns to June
370 2016, and the wavelength composition of the knickpoint remains stable while migrating
371 up the channel, with the whole unit (knickpoint and the associated downstream
372 crescentic bedforms) being elongated. A few extremely long-wavelength (up to 120 m)
373 bedforms are present and extend to 400 m, downstream of the knickpoint.

374

375 **Sedimentary record of turbidity currents over a knickpoint**

376 Cores obtained from the central axis of the channel (see Fig. 9B for locations and
377 context) over the closely studied knickpoint show that the highly active channel is a
378 predominantly sandy system, reworked by repeated turbidity currents (Fig. 9B). Some
379 of the sediment cores may have been disturbed during the coring process due to tube
380 friction, resulting in convex deformation of the lamination (for example, STN009 and
381 STN010). Contacts between beds are generally sharp and erosive, with erosional
382 discontinuities in STN007 and STN018. Sediments in the cores can be correlated via
383 comparison with the bathymetric difference maps. All sediment cores downstream of
384 the knickpoint, collected in the October 2016 survey, were deposited between June

and October 2016, most likely by the last few larger flows that passed ADCP5 and ADCP4 during 2016 (Figs 2A and 9A). A layer of light-grey mud (1 to 2 cm) distinct from the darker-grey mud layers in the deeper sections of cores is seen at the very top of sediment cores, likely representing background hemipelagic deposition or the late waning stage deposits of the previous turbidity current.

Core STN017, situated upstream of the knickpoint head, is composed of coarse sand fining upward to medium/fine sand, showing a relatively minor change in grain size. (Fig. 9A and B). At a similar location, piston core STN007 was collected during the June 2016 survey and the core length is around seven times longer than core STN017, presenting better developed textural grading from very coarse to fine sand. Core STN016 features well-developed cross-stratification. At the toe of the knickpoint, core STN015 sampled a sandy bed comprising woody organic fragments at the top. Interbedded sand and mud laminations are present at STN009 and STN010 which are located just downstream of the knickpoint. The dark-grey mud layer within the sand-mud laminations likely settled in the wake of the flows. Each lamina in core STN009 contains an upward-fining sand layer and a dark mud/silty layer (typical turbidites). Farther down the system, cores STN014 and STN018 present a normally-graded sand sequence with a mud cap. Compared to STN009 and STN010, the muddy sections of STN014 and STN018 could have all been eroded (or may not have been deposited homogenously), with the exception of the very last mud drape. The aggradation just downstream of the knickpoint is thicker than farther down system over the study period (see Fig. 9A), likely related to rapid fallout of sand eroded from the knickpoint face.

DISCUSSION

Characterizing the seafloor morphology of the submarine channel

A recent study of Bute Inlet by Heijnen *et al.* (2020) demonstrated how exceptionally fast-moving and internally-generated knickpoints dominate the evolution of the submarine channel and cause channel-wide erosion, potentially resulting in channel geometry asymmetry and lateral migration of the channel thalweg. Turbidity currents transport sediment eroded by upstream knickpoint migration and deposit them downstream of knickpoint and even farther down channel, which exerts a strong control on the erosion and deposition pattern of the overall submarine channel system. The bathymetric surveys and wavelet analyses indicate that the entire submarine channel is composed of a train of knickpoints with superimposed higher frequency crescentic bedforms. Previous observations have shown how similar crescentic bedforms are eroded and migrate upslope due to hydraulic jumps within supercritical turbidity currents (Hughes Clarke, 2016; Hage *et al.*, 2018). Crescentic bedforms are omnipresent along the two deltaic clinoforms, with bedform wavelengths varying from 10 to 50 m and with heights from 0.2 to 2.5 m. The generally higher values of bedform height and wavelength in the Homathko October 2016 survey data compared to the November 2018 survey data might be related to the lower river discharge in 2018 than in 2016 (Canadian Hydrographic Office). As the channel becomes deeper and the channel gradient declines distally, a train of knickpoints is formed along the main channel system that have smaller-scale superimposed crescentic bedforms with dominant wavelengths varying from *ca* 16 to *ca* 128 m. The scale of bedform wavelength changes over knickpoint features and their dynamics appear to be closely coupled. The authors posit that as flows pass over the steep knickpoint face, they accelerate; the downstream effect of which serves to modify the scale of crescentic bedforms created by the flows. The extent of that modification is therefore likely a function of the distance over which elevated flow velocity is maintained. However,

435 more work is needed to quantify the possible relationships between knickpoint
436 gradients, bedform dimensions and the formative currents.

437 In addition, the variation in the length of the zone downstream of knickpoints, within
438 which crescentic bedforms are superimposed, may suggest that hydrodynamic
439 differences in the interaction between knickpoints and turbidity currents can induce a
440 variability in the spatial and temporal distribution of the crescentic bedforms. This has
441 important implications because these zones immediately downstream of knickpoints
442 are likely sites of higher preservation potential for deposits accumulated by turbidity
443 currents. Thus variations in the size and distribution of bedforms deposited within this
444 region, particularly if they are significant along the overall extent of the channel bed,
445 might prove a key factor to explore process–product relationships in these systems.
446 Such variability would need to be included in new models (e.g. Hage *et al.*, 2018) and
447 allow for alterations in the thickness of crescentic bedforms to be accounted for.

448 The variability of knickpoints and bedforms will also impact bed roughness. Bed
449 roughness is an essential parameter for the understanding of hydrodynamics and
450 sediment dynamics in sedimentary systems (Kleinhans, 2005; Lefebvre *et al.*, 2011;
451 Dorrell *et al.*, 2013). Due to the large dimensions and wide distribution of knickpoints
452 and associated crescentic bedforms, these compound seabed morphologies exert a
453 strong local impact on flow dynamics and evolution and on sediment transport in
454 overlying turbidity currents. Since the dimension and size of knickpoints and crescentic
455 bedforms vary from the proximal portions of the channel to the distal lobe, bedform
456 roughness of the channel seafloor will change accordingly. Channel depth (i.e. depth
457 from channel seabed to levee top) generally decreases from *ca* 35 m proximally to a
458 few metres at the outlet adjoining distal lobe, with a few locally deepened erosion
459 zones along the channel (Heijnen *et al.*, 2020). Most of the turbidity currents captured

460 in the ADCP data dissipated within the upper channel, and only three turbidity currents
461 reached the end of the instrument array (Fig. 2A). The often-powerful nature of turbidity
462 currents can significantly modify the channel seafloor morphology (Hughes Clarke,
463 2016; Paull *et al.*, 2018). Therefore, the bedform roughness variation along the
464 channel seafloor suggests corresponding changes in the Chézy coefficient (the
465 relation between friction on flow boundary and flow velocity) longitudinally along the
466 system, as well as changes in its impact on bed shear stress and turbidity current
467 hydrodynamics (for example, shear velocity, turbulence and suspended sediment
468 concentration). Although a range of empirical formulae have been developed to
469 estimate roughness in unidirectional riverine flow (Swart, 1976; Grant & Madsen, 1982;
470 Van Rijn, 1984; Nielsen, 1992; Soulsby, 1997), there remains debate on how to best
471 quantify bedform roughness in submarine environments. Further investigation is
472 needed to quantitatively understand how flows evolve along submarine channels
473 based on seabed morphology, and to constrain the effects of changing Chézy
474 coefficient on currents crossing the system. For example, further study of the role of
475 roughness on the runout distance of turbidity currents will provide significant advances
476 to understanding and predicting how such currents evolve down-system, thus
477 providing additional insights for the interpretation of their sedimentary deposits.

478

479 **Role of slope gradient on controlling channel morphological features**

480 This section explores how seabed gradient affects knickpoints and bedforms. Similar
481 scales of knickpoints and superimposed crescentic bedforms have been observed in
482 the seafloor of Monterey Canyon (offshore California, USA) and the upper part of the
483 Capbreton submarine canyon (offshore western France), which maintain a longitudinal
484 gradient of 1.6° and 1.0° respectively (Paull *et al.*, 2011; Guiastrennec-Faugas *et al.*,

2020). The South Taiwan Shoal and West Penghu submarine canyons in the South China Sea also host a series of large-scale features that can be interpreted as knickpoints, ranging in average gradient from 0.26° to 1.24° (Zhong *et al.*, 2015). In this study, knickpoints start to form at *ca* 7 km from the Homathko Delta lip. The knickpoints extend to the distal channel across an average slope varying from 1.0° to 0.25°, a similar gradient to the features observed in canyons of the South China Sea. Knickpoint formation in Bute Inlet occurs in a system with a similar seabed gradient to other locations, and therefore knickpoint formation could indeed be a function of slope. Previous research has reviewed bedform features which are morphologically similar to crescentic bedforms, termed cyclic steps. Cyclic steps are defined as a type of upper-flow-regime bedforms consisting of trains of upstream-migrating and upslope-migrating bed undulations (Slootman & Cartigny, 2020), although such upper-stage flow regime conditions are likely not a prerequisite for the formation of all crescentic bedforms (Paull *et al.*, 2010). Slope controls on cyclic steps have been noted by previous research, such as the Monterey East Channel (0.61°; Fildani *et al.*, 2006), the Eel Canyon (1.61°; Lamb *et al.*, 2008), the Redondo Fan Valley (1.28°-2.09°; Normark *et al.*, 2009) and the San Mateo Channel (1.94°; Covault *et al.*, 2014). Kostic (2011), on the basis of numerical simulations, suggested that cyclic steps could not form on higher slope gradients. Crescentic bedforms formed in the Squamish Delta have been interpreted as cyclic steps based on direct flow-monitoring data (Hughes Clarke, 2016). In this study, crescentic bedforms present at both deltas are morphologically similar to the bedforms in the Squamish Delta and thus the authors infer that these crescentic bedforms are cyclic steps. The slope gradient of both deltas is up to 8°, which indicates that cyclic steps could be formed at relatively steep slope gradients. Therefore, the model from Kostic (2011) may be applicable to a wider range

of systems than previously thought. Additionally, prior research proposed that slope gradient controls the aspect ratio (ratio of bedform wavelength to height) of the bedforms (Normandeau *et al.*, 2016; Dietrich *et al.*, 2016); however, the present study shows that river discharge could also influence the aspect ratio of crescentic bedforms, as is evident from the bathymetric changes in the Homathko Delta in 2016 and 2018 (Fig. 6C).

A new model of the interaction between turbidity currents, knickpoints and crescentic bedforms

Turbidity current structure and the associated depositional signature have drawn significant attention in the last decades (e.g. Walker, 1967; Komar, 1985; Sumner *et al.*, 2013; Postma & Cartigny, 2014; Paull *et al.*, 2018) and their sedimentary deposits play a significant role in current understanding of turbidity-current flow dynamics and evolution (e.g. Kuenen & Migliorini, 1950; Pirmez & Imran, 2003; Talling *et al.*, 2012; Hubbard *et al.*, 2014). Hage *et al.* (2018) has identified sedimentary architectures related to back-stepping bedforms and scour fills in the delta front. Sediment cores enable the deciphering of depositional processes and the sedimentary environment from which the stratigraphic evolution associated with turbidity currents can be reconstructed. The flow monitoring, repeat seafloor surveys and a series of sediment cores are now integrated, to present a new model for the depositional architecture and sedimentary facies that occur across a knickpoint, with specific reference to the interactions between the knickpoint, crescentic bedforms and the successive flows that drive their upstream migration (Fig. 10).

Phase (1): Slow-moving turbidity current upslope of the knickpoint

The channel bed surface gradient is relatively low between adjacent knickpoints (typically 0.12 to 0.27 degrees), and the turbidity-current frontal speed is thus reasoned to be relatively slower upslope of the knickpoint.

Phase (2): Acceleration of the turbidity current over the knickpoint

Large-scale crescentic bedforms (in terms of height and wavelength) are superimposed on the knickpoint and are altered during knickpoint retreat, clustering around and tracking the knickpoints spatially. Bedform morphologies on the high-gradient leeside of the knickpoint are related to flow acceleration over the knickpoint, and could indicate the presence of a supercritical flow region. Low levels of mud preservation occur within cores recovered from the steep face of the knickpoint. Mud layers deposited in the wake of the flow, and from settling of hemipelagic sediments, are unlikely to be preserved in the bedform region associated with the knickpoint; this is due to entrainment by successive flows.

Phase (3): Potential hydraulic jump

The deposition of large sand volumes (i.e. core STN015) is possibly linked to flow deceleration at the transition from supercritical to subcritical over the knickpoint, leading to rapid settling of sand from suspension in a region just downstream of the knickpoint. The transition from net-erosion to net-deposition in Fig. 9 is the region where a hydraulic jump may have occurred (i.e. at *ca* 500 m in Fig. 9A).

Phase (4): Decrease in bedform wavelength with distance downstream of the knickpoint

Farther downstream of the knickpoint, bedform wavelengths gradually decrease to smaller scales similar to bedforms in Phase (1). The deposits of sand-mud lamination due to flow deceleration indicate higher preservation potential.

Phase (5): Downslope deposition of sediment

In the downslope region, typically over thousands of metres distance from the previous knickpoint (and upslope of the next knickpoint), aggradation gradually decreases down-channel. Turbidity currents primarily deposit sand overlain by a mud cap. It could be inferred that the mud layer is easily eroded and entrained by a successive flow and thus the mud may play a role in sustaining turbidity currents over the shallow gradients between knickpoints.

Cyclic steps are bounded by local flow transitions from supercritical to subcritical states (Kostic & Parker, 2006; Slootman & Cartigny, 2020). Sediment cores, collected over crescentic bedforms that are interpreted as cyclic steps at Squamish Delta (Hughes Clarke, 2016; Covault *et al.*, 2017), reveal multiple units of ungraded or poorly graded sandy deposits without a regular top mud layer and lamination (Hage *et al.*, 2018). In this study, deposits do show mud and sand beds as part of the depositional signature; however, these tend to be located within specific zones that are clustered downstream of knickpoints. Previous work has suggested trends in grain-size and facies variation downstream of knickpoints (Postma & Cartigny, 2014); however such a trend is not observed here. Possible reasons for the absence of such a trend could be: (i) sampling bias due to preferential sampling of the shallow surface sediments in this study, thus not capturing deeper part of the sediments; (ii) the possible role of different flow magnitudes in producing different facies signatures; and (iii) the possibility that the depositional model of Postma & Cartigny (2014) may be inadequate as a generalization;

The amount of aggradation immediately downstream of a knickpoint is greater than farther down-slope, suggesting a better preservation potential at this position over at least short timescales (Fig. 9A). This rapid deposition indicates that most of the sand

583 eroded locally at the knickpoint rapidly falls out of suspension just downstream of the
584 knickpoint. The lack of mud layers suggests that the flows are likely sustained by the
585 mobilization of fluid-mud layers (the uncompacted mud layer rich in water) on the
586 seafloor, rather than by the basal sand. The regions downstream of knickpoints will
587 likely dominate in terms of the preservation in submarine channel deposits due to
588 higher aggradation rate and better preservation potential at these specific locations.
589 Therefore such variability, and the space–time coupling of knickpoints and crescentic
590 bedform interactions, need to be better integrated into our conceptual
591 sedimentological models for these systems.
592
593 **CONCLUSIONS**
594 The geomorphology of submarine channel knickpoints and associated crescentic
595 bedforms have been analysed in unusual detail within Bute Inlet, western Canada,
596 using a combination of bathymetric measurements, sediment cores and acoustic
597 Doppler current profiler data. The results of wavelet analysis on the bathymetric data
598 reveal distinct trends and a specific spatial-temporal coupling between the larger
599 knickpoint features and superimposed crescentic bedforms. Due to the variable
600 dimensions of knickpoints and associated crescentic bedforms, bedform roughness
601 and its systematic variation along the channel seafloor potentially exert a significant
602 influence on turbidity-current hydrodynamics and runout, which remains an avenue for
603 future research. Analyses of sediment cores suggest that deposits accumulated in
604 regions immediately downstream of knickpoints will likely dominate the preservation
605 within submarine channel systems. This shows why a detailed examination of the
606 coupling between knickpoints and crescentic bedforms is needed to inform a process–
607 product understanding for these subaqueous systems affected by turbidity currents.

ACKNOWLEDGEMENTS

We thank the captains and crews of *R/V Strickland* and *CCGS Vector* as well as the support team in Bear Lodge, Bute Inlet. The field campaign was supported by Natural Environment Research Council Grants NE/M007138/1 and NE/M017540/1. C. Y. was funded by the China Scholarship Council and the University of Hull. D. R. P. acknowledges funding received from the European Research Council under the European Union's Horizon 2020 research and innovation program (Grant Agreement 725955). M. J. B. C. was funded by a Royal Society Research Fellowship. M. A. C. was supported by the U.K. National Capability NERC CLASS program (NERC Grant NE/R015953/1) and NERC Grants (NE/P009190/1 and NE/P005780/1). The authors declare no conflicts of interest. Finally, we thank Arnoud Slootman, Alessandro Cantelli, Shaoru Yin, Dario Ventra and an anonymous reviewer for the quality of their reviews, which has significantly enhanced the quantity of the final manuscript.

DATA AVAILABILITY STATEMENT

Data related to this paper are available online at “NOAA data repository” (https://accession.nodc.noaa.gov/0202076).

628 # REFERENCES

629 **Azpiroz-Zabala, M., Cartigny, M.J.B., Talling, P.J., Parsons, D.R., Sumner, E.J., Clare, M.A.,**
630 **Simmons, S.M., Cooper, C.,** and **Pope, E.L.** (2017) Newly recognized turbidity currents structure
631 can explain prolonged flushing of submarine canyons. *Science Advances*., **3**, e1700200.

632 **Babonneau, N., Delacourt, C., Cancouët, R., Sisavath, E., Bachèlery, P., Mazuel, A., Jorry, S.J.,**
633 **Deschamps, A., Ammann, J.** and **Villeneuve, N.** (2013) Direct sediment transfer from land to
634 deep-sea: insight into shallow multibeam bathymetry at La Réunion Island. *Mar. Geol*., **346**, 47-
635 57.

636 **Baynes, E.R.C., Lague, D., Attal, M., Gangloff, A., Kirstein, L.A.** and **Dugmore, A.J.** (2018) River
637 self-organisation inhibits discharge control on waterfall migration. *Sci. Rep*., **8**, 2444.

638 **Bornhold, B.D., Ren, P.** and **Prior, D.B.** (1994) High-frequency turbidity currents in British Colombia
639 fjords. *Geo-Mar. Lett*., **14**, 238–243.

640 **Bouma, A.H.** (2000) Coarse-grained and fine-grained turbidite systems as end member models:
641 applicability and dangers. *Mar. Pet. Geol*., **17**,137-143.

642 **Bennett, S**. and **Best, J.** (1995) Mean flow and turbulence structure over fixed, two-dimensional dunes:
643 implications for sediment transport and bedform stability. *Sedimentology* **42**, 491-513.

644 **Best, J.** (2005b) Kinematics, topology and significance of dune-related macroturbulence: some
645 observations from the laboratory and field. *Fluvial Sedimentology VII.,* **35**, 41-60.

646 Canadian Hydrographic Office, data available from https://wateroffice.ec.gc.ca/.

647 **Cantelli, A.** and **Muto, T.** (2014) Multiple knickpoints in an alluvial river generated by a single
648 instantaneous drop in base level: experimental investigation. *Earth Surf. Dyn.,* **2**, 271-278.

649 **Carter, L., Gavey, R., Talling, P.J.** and **Liu, J.T.** (2014) Insights into submarine geoharzards from
650 breaks in subsea telecommunication cables. *Oceanography.,* **27**, 58-67.

651 **Cartigny, M.J.B., Ventra, D., Postma, G.** and **van Den Berg, J.H.** (2014) Morphodynamics and
652 sedimentary structures of bedforms under supercritical-flow conditions: New insights from flume
653 experiments. *Sedimentology.,* **61**, 712-748.

654 **Clare, M.A., Hughes Clarke, J.E., Talling, P.J., Cartigny, M.J.B.** and **Pratomo, D.G.** (2016)
655 Preconditioning and triggering of offshore slope failures and turbidity currents revealed by most
656 detailed monitoring yet at a fjord-head delta. *Earth Planet. Sci. Lett*., **450**, 208-220.

657 **Clare, M.A., Lintern, D.G., Rosenberger, K., Hughes Clarke, J.E., Paull, C., Gwiazda, R., Cartigny,**

M.J.B., Talling, P.J., Perara, D., Xu, J.P., Parsons, D.R., Silva Jacinto, R. and **Apprioual. R.** (2020) Lessons learned from the monitoring of turbidity currents and guidance for future platform designs. *Geo. Soc. London Special Pub*., **500**, 605-634.

Conway, K.W., Barrie, J.V., Picard, K. and **Bornhold, B.D.** (2012) Submarine channel evolution: active channels in fjords, British Columbia, Canada. *Geo-Mar. Lett*., **32**, 301-312.

Cooper, C., Wood, J. and **Andrieux, O.** (2013) Turbidity current measurements in the Congo Canyon. Offshore Technology Conference, Houston, TX, 6 - 9 May 2013.

Covault, J.A., Kostic, S., Paull, C.K., Ryan, H.F. and **Fildani, A.** (2014) Submarine channel initiation, filling and maintenance from sea-floor geomorphology and morphodynamics modelling of cyclic steps. *Sedimentology*., **61**, 1031-1054.

Covault, J.A., Kostic, S., Paull, C.K., Sylvester, Z. and **Fildani, A.** (2017) Cyclic steps and related supercritical bedforms: Building blocks of deep-water depositional systems, western North America. *Mar. Geol.* **393**, 4-20.

Dietrich, P., Ghienne, J-F., Normandeau, A. and **Lajeunesse, P.** (2016) Upslope-migrating bedforms in a proglacial sandur delta: Cyclic steps from river-derived underflows? *J. Sediment. Res.,* **86**, 112-122.

Dorrell, R.M., Darby, S.E., Peakall, J., Sumner E.J., Parsons, D.R. and **Wynn, R.B.** (2013) Superelevation and overspill control secondary flow dynamcis in submarine channels. *JGR Oceans.,* **118**, 3895-3915.

Englert, R.G., Hubbard, S.M., Cartigny, M.J.B., Clare, M.A., Coutts, D.S., Hage, S., Hughes Clarke, J.E., Jobe, Z., Lintern, D.G., Stacey, C. and **Vendettuoli D.** (2020) Quantifying the three-dimensional stratigraphic expression of cyclic steps by integrating seafloor and deep-water outcrop observation. *Sedimentology*.

Fildani, A., Normark, W.R., Kostic, S. and **Parker, G.** (2006) Channel formation by flow stripping: large-scale scour features along the Monterey East Channel and their relation to sediment waves. *Sedimentology.,* **53**: 1265-1287.

Gales, J.A., Talling, P.J., Cartigny, M.J.B., Clarke, J.H., Lintern, G., Stacey, C. and **Clare, M.A.** (2019) What controls submarine channel development and the morphology of deltas entering deep-water fjords? *Earth Surf. Processes Landf.,* **44**, 535-551.

Gilbert, G.K. (1895) Niagara Falls and their history. National Geographic Society. The Physiography

of the United States. The American Book Co., New York., 203-236.

Girardclos, S., Hilbe, M., Corella, J.P., Loizeau, J-L., Kremer, K., Delsontro, T., Arantegui, A., Moscariello, A., Arlaud, F., Akhtman, Y., Anselmetti, F.S. and **Lemmin, U.** (2012) Searching the Rhone delta channel in Lake Geneva since François‐Alphonse Forel. *Archives des Sciences.,* **65**, 103-118.

Grant, W.D. and **Madsen, O.S.** (1982) Movable bed roughness in oscillatory flow. *J. Geophys. Res.,* **87**, 469-481.

Guiastrennec-Faugas, L., Gillet, H., Jacinto, R.S., Dennielou, B., Hanquiez, V., Schmidt, S., Simplet, L. and **Rousset, A.** (2020) Upstream migrating knickpoints and related sedimentary processes in a submarine canyon from a rare 20-year morphobathymetric time-lapse (Capbreton submarine canyon, Bay of Biscay, France). *Mar. Geol.*, **423**, 106143.

Gutierrez, R.R., Abad, J.D., Parsons, D.R. and **Best, J,L.** (2013) Discrimination of bed form scales using robust spline filters and wavelet transforms: Methods and application to synthetic signals and bed forms of the Río Paraná, Argentina. *J. Geophys. Res. Earth Surface*., **118**, 1400-1419.

Gutierrez, R.R., Mallma, J.A., Núñez-González, F., Link, O. and **Abad, J.D.** (2018) Bedforms-ATM, an open source software to analyse the scale-based hierarchies and dimensionality of natural bedforms. *SftwareX*., **7**, 184-189.

Hage, S., Cartigny, M.J.B., Clare, M.A., Sumner, E.J., Vendettuoli, D., Hughes Clarke, J.E., Hubbard, S.M., Talling, P.J., Lintern, G., Stacey, C.D., Englert, R.G., Vardy, M.E., Hunt, J.E., Yokokawa, M., Parsons, D.R., Hizzett, J.L., Azpiroz-Zabala, M. and **Vellinga, A.J.** (2018) How to recognize crescentic bedforms formed by supercritical turbidity currents in the geological records: Insight from active submarine channels. *Geology*., **46**, 563-566.

Hage, S., Cartigny, M.J.B., Sumner, E.J., Clare, M.A., Hughes Clarke, J.E., Talling, P.J., Lintern, D.G., Simmons, S.M., Silva Jacinto, R., Vellinga, A.J., Allin, J.R., Azpiroz-Zabala, M., Gales, J.A., Hizzett, J.L., Hunt, J.E., Mozzato, A., Parsons, D.R., Pope, E.L., Stacey, C.D., Symons, W.O., Vardy, M.E. and Watts, C. (2019) Direct Monitoring reveals initiation of turbidity currents from extremely dilute river plumes. *Geophys. Res. Lett.,* **46**, 11310-11320.

Hayakawa, Y. and Matsukura, Y. (2003) Recession rates of waterfalls in Boso Peninsula, Japan, and a predictive equation. *Earth Surf. Processes and Landf.,* **28**: 675-684.

Heijnen, M.S., Clare, M.A., Cartigny, M.J.B., Talling, P.J., Hage, S., Lintern, G., Stacey, C., Parsons, D.R., Simmons, S.M., Chen, Y., Sumner, E.J., Dix, J.K. and **Hughes Clarke, J.E.** (2020)

719 Rapidly-migrating and internally-generated knickpoints can control submarine channel evolution.
720 *Nature Communications.*, **11**, 3129.
721 **Hizzett, J.L., Hughes Clarke, J.E., Sumner, E.J., Cartigny, M.J.B., Talling, P.J.** and **Clare, M.A.**
722 (2017) Which triggers produce the most erosive, frequent and longest runout turbidity currents on
723 deltas? *Geophys. Res. Lett.,* **45**, 855-863.
724 **Holland, W.N.** (1974) Origin and development of hanging valleys in the Blue Mountains, New South
725 Wales. Ph.D. Thesis, Sydney University, Sydney, Australia, 416.
726 **Hubbard, S.M., Covault, J.A., Fildani, A.** and **Romans, B.W.** (2014) Sediment transfer and
727 deposition in slope channels: Deciphering the record of enigmatic deep-sea processes from
728 outcrop. *Geol. Soc. Am. Bull.,* **126**, 857-871.
729 **Hughes Clarke, J.E., Brucker, S., Muggah, J., Church, I., Cartwright, D., Kuus, P., Hamilton, T.,**
730 **Pratoma, D.** and **Eisan, B.** (2012) The Squamish prodelta: monitoring active landslides and
731 turbidity currents. Canadian Hydrographic Conference, 15.
732 **Hughes Clarke, J.E., Vidiera Marques, C.R.** and **Pratomo, D.** (2014) Imaging active mass-wasting
733 and sediment flows on a fjord delta, Squamish, British Columbia. Submarine Mass Movements
734 and Their Consequences, **37**, 249-260.
735 **Hughes Clarke, J.E.** (2016) First wide-angle view of channelized turbidity currents links migrating cyclic
736 steps to flow characteristics. *Nat. Commun.,* **7**, 11896.
737 **Inman, D.L., Nordstrom, C.E**. and **Flick, R.E.** (1976) Currents in submarine canyons: an air-sea-land
738 interaction. *Annual Review of Fluid Mechanic.,* 8, 275-310.
739 **Khripounoff, A., Vangriesheim, A., Crassous, P.** and **Etoubleau, J.** (2009) High frequency of
740 sediment gravity flow events in the Var submarine canyon (Mediterranean Sea). *Mar. Geol.,* **263**,
741 1-6.
742 **Kleinhans, M.G.** (2005) Flow discharge and sediment transport models for estimating a minimum
743 timescale of hydrological activity and channel and delta formation of Mars. *J. Geophys. Res.,* **110**.
744 **Komar, P.D.** (1985) The hydraulic interpretation of turbidites from their grain sizes and sedimentary
745 structures. *Sedimentology.*, **32**, 395–407.
746 **Kostaschuk, R.** (2006) Sediment transport mechanics and subaqueous dune morphology, River,
747 Coastal and Estuarine Morphdynamics. London, Taylor and Francis Group, 795-801.
748 **Kostic, S.** and **Parker, G.** (2006) The response of turbidity currents to a canyon-fan transition: internal

749 hydraulic jumps and depositional signature. *J. Hydraul. Res.,* **44**, 631-653.
750 **Kostic, S.** (2011) Modeling of submarine cyclic steps: Controls on their formation, migration, and
751 architecture. *Geosphere*, **7**, 294-304.
752 **Kostic, S.** (2014) Upper flow regime bedforms on levees and continental slopes: Turbidity current flow
753 dynamics in response to fine-grained sediment waves. *Geosphere*., **10**, 1094-1103.
754 **Kuenen, Ph.H.** and **Migliorini, C.I.** (1950) Turbidity currents as a cause of graded bedding. *Geology*.,
755 **58**, 91-127**.**
756 **Lamb, M.P., Parsons, J.D., Mullenbach, B.L., Finlayson, D.P., Orange, D.L.,** and **Nittrouer, C.A.**
757 (2008) Evidence for superelevation, channel incision, and formation of cyclic steps by turbidity
758 currents in Eel Canyon, California. *Geol. Soc. Am. Bull.*, **120**, 463-475,
759 **Lefebvre, A., Erstsen, V.B.** and **Winter, C.** (2011) Influence of compound bedforms on hydraulic
760 roughness in a tital environment. *Ocean Dyn.,* **61**, 2201-2210.
761 **Leyland, J., Hackney, C.R., Darby, S.E., Parsons, D.R., Best, J.L., Nicholas, A.P., Aalto, R.** and
762 **Lague, D.** (2016) Extreme flood-driven fluvial bank erosion and sediment loads: direct process
763 measurements using integrated Mobile Laser Scanning (MLS) and hydro-acousitc techniques.
764 *Earth Surf. Process Landf.,* **42**, 334-346.
765 **Masson, D.G., Kenyon, N.H., Gardner, J.V.** and **Field, M.E.** (1995) Monterey Fan: channel and
766 overbank morphology. Atlas of Deep Water Environments, Architectural style in turbidite system,
767 Pickering KT, Hiscott RN, Kenyon NH, Ricci Lucchi F, Smith RDA (Eds), 74-79.
768 **Mitchell, N.C.** (2006) Morphologies of knickpoints in submarine canyons. *Geol. Soc. Am. Bull.,*
769 **118**, 589-605.
770 **Mulder, T., Syvitski, J.P.M., Migeon, S., Faugeres, J.C.,** and **Savoye, B.** (2003) Marine hyperpycnal
771 flows: initiation, behavior and related deposits. A review. *Mar. Pet. Geol.,* **20**, 861-882.
772 **Nielsen, P.** (1992) Coastal bottom boundary layers and sediment transport. *Advanced Series on Ocean*
773 Eng., 4.
774 **Normark, W.R., Piper, D.J.W., Posamentier, H., Pirmez, C.** and **Migeon, S.** (2002) Variability in form
775 and growth of sediment waves on turbidite channel levees. *Mar. Geol.,* **192**, 23-58.
776 **Normark, W.R., Paull, C.K., Caress, D.W., Ussler, W., III,** and **Sliter, R.** (2009) Fine-scale relief
777 related to late Holocene channel shifting within the fl oor of the upper Redondo Fan, offshore
778 Southern California. *Sedimentology*., **56**, 1690-1704.

779 **Normandeau, A., Lajeunesse, P., St-Onge, G., Bourgault, D., St-Onge Drouin, S., Senneville, S.**
780 and **Bélanger, S.** (2014) Morphodynamics in sediment-starved inner-shelf submarine canyons
781 (Lower St. Lawrence Estuary, Eastern Canada). *Mar. Geol.,* **357**, 243-255.
782 **Normandeau, A., Lajeunesse, P.** and **St-Onge, G.** (2015) Submarine canyons and channels in the
783 Lower St. Lawrence Estuary (Easter Canada): Morphology, classification and recent sediment
784 dynamics. *Geomorphology.,* **241**, 1-18.
785 **Normandeau, A., Lajeunesse, P., Poire, A.G.** and **Francus, P.** (2016) Morphological expression of
786 bedforms formed by supercritical sediment density flows on four fjord-lake deltas of the south-
787 eastern Canadian Shield (Eastern Canada). *Sedimentology*, **63**, 2106-2129.
788 **Obelcz, J., Xu, K.H., Georgiou, I.Y., Maloney, J., Bentley, S.J.** and **Miner, M.D.** (2017) Sub-decadal
789 submarine landslides are important drivers of deltaic sediment flux: Insights from the Mississippi
790 River Delta front. *Geology.,* **45**, 703-706.
791 **Parsons, J.D., Bush, J.W.M.** and **Syvitski, J.P.M.** (2001) Hyperpycnal plume formation from riverine
792 outflows with small sediment concentrations. *Sedimentology.,* **48**, 465-478.
793 **Parsons, D.R., Best, J.L., Orfeo, O., Hardy, R.J., Kostaschuk, R.** and **Lane, S.N.** (2005) Morphology
794 and flow fields of three-dimensional dunes, Rio Paraná Argentina: Results from simultaneous
795 multibeam echo sounding and acoustic Doppler current profiling. *J. Geophys. Res.,* **110**.
796 **Paull, C.K., Ussler, W., Caress, D.W., Lundsten, E., Covault, J.A., Maier, K.L., Xu, J.P.** and
797 **Augenstein, S.** (2010) Origins of large crescent-shaped bedforms within the axial channel of
798 Monterey Canyon, offshore California. *Geosphere.,* **6**, 755-774.
799 **Paull, C.K., Caress, D.W., Ussler, W., Lundsten, E.** and **Meiner-Johnson, M.** (2011) High-resolution
800 bathymetry of the axial channels within Monterey and Soquel submarine canyons, offshore central
801 California. *Geosphere.,* **7**, 1077-1101. https://doi.org/10.1130/GES00636.1
802 **Paull, C.K., Talling, P.J., Katherine, L.M., Parsons, D.R., Xu, J.P., Caress, D.W., Gwiazda, R.,**
803 **Lundsten, E.M., Anderson, K., Barry, J.P., Chaffey, M., O'Reilly, T., Rosenberger, K.J., Gales,**
804 **J.A., Kieft, B., McGann, M., Simmons, S.M., McCann, M., Sumner, E.J., Clare, M.A.** and
805 **Cartigny, M.J.** (2018) Powerful turbidity currents driven by dense basal layers. *Nat. Commun.,* **9**,
806 4114.
807 **Peakall, J., Amos, K.J., Keevil, G.M., William Bradbury, P.** and **Gupta, S.** (2007) Flow processes
808 and sedimentation in submarine channel bends. *Mar. Pet. Geol.,* **24**, 470-486.

Peakall, J. and **Sumner, E.J.** (2015) Submarine channel flow processes and deposits: A process-product perspective. *Geomorphology*., **244**, 95-120.

Pederson, J.L. and **Tressler C.** (2012) Colorado River long-profile metrics, knickzones and their meaning. *Earth and Planetary Science Letters.,* **345-348**, 171-179.

Piper, D.J.W., Cochonat, P. and **Morrison, M.L.** (1999) The sequence of events around the epicentre of the 1929 Grand Banks earthquake: initiation of debris flows and turbidity currents inferred from sidescan snoar. *Sedimentology.,* **46**, 79-97.

Pirmez, C. and **Imran, J.** (2003) Reconstruction of turbidity currents in Amazon Channel. *Mar. Pet. Geol.*, **20**, 823-849.

Postma, G. and **Cartigny, M.J.B.** (2014) Supercritical and subcritical turbidity currents and their deposits-A synthesis. *Geology*., **42**, 987-990.

Pomar, L., Morsilli, M., Hallock, P. and **Badenas, B.** (2012) Internal waves, an under-explored source of turbulence events in the sedimentary record. *Earch. Sci. Rev.,* **111**, 56-81.

Prior, D.B., Wiseman, W.J. and **Gilbert, R.** (1981) Submarine slope processes on a fan delta, Howe Sound, British Columbia. *Geo. Mar. Lett.,* **1**, 85-90.

Prior, D.B. Bornhold, B.D., Wiseman, W.J. and **Lowe, D.R.** (1987) Turbidity current activity in a British Columbia Fjord. *Science*., **237**, 1330-1333.

Puig, P., Ogston, A.S., Mullenbach, B.L., Nittrouer, C.A., Parsons, J.D. and **Sternberg, R.W.** (2004) Storm-induced sediment gravity flows at the head of the Eel submarine canyon, northern California margin. *J. Geophys. Res. Oceans.*, **109**.

Ressink, A.J.H. and **Bridge, J.S.** (2011) Evidence of bedform superimposition and flow unsteadiness in unit-bar deposits, South Saskatchewan River, Canada. *J. Sediment. Res.,* **81**, 814-840.

Shao, D.L., Fan, G.Z., Wang, H.Q., Ma, H.X., Zuo, G.P., Ding, L.B., Cai, Z. and **Li, W.Q.** (2021) 3D anatomy and flow dynamics of net-depositional cyclic steps on the world's largest submarine fan: a joint 3D seismic and numerical approach. *Petroleum Sicence,* **18**, 10-28.

Slootman, A. and **Cartigny, M.J.B.** (2020) Cylic steps: Review and aggradation-based classification. *Earth. Sci. Rev.,* **201**, 102949.

Simmons, S.M., Azpiroz_Zabala, M., Cartigny, M.J.B., Clare, M.A., Parsons, D.R., Pope, E.L., Sumner, E.J. and **Talling, P.J.** (2020) Novel acousitc method provides first detailed measurements of sediment concentration structure within submarine turbidity currents. *JGR,*

839 *Oceans.,* **125**, e2019JC015904.

840 **Smith, D.P., Ruiz, G., Kvitek, R.** and **Lampietro, P.J.** (2005) Semiannual patterns of erosion and
841 deposition in upper Monterey Canyon from serial multibeam bathymetry. *Geol. Soc. Am. Bull.,*
842 **117**, 1123–1133.

843 **Smith, D.P., Kvitek, R., Lampietro, P.J.** and **Wong, K.** (2007) Twenty-nine months of geomorphic
844 change in upper Monterey Canyon (2002-2005). *Mar. Geol.,* **236**, 79-94.

845 **Soulsby, R.L.** (1997) Dynamics of marine sands: a manual for practical applications. Thomas Telford,
846 London.

847 **Sumner, E.J., Peakall, J., Parsons, D.R., Wynn, R.B., Darby, S.E., Dorrell, R.M., McPhail, S.D,,**
848 **Perrett, J., Webb, A.** and **White, D.** (2013) First direct measurements of hydraulic jumps in an
849 active submarine density current. *Geophys. Res. Lett.,* **40**, 5904-5908.

850 **Swart, D.H.** (1976) Predictive equations regarding coastal transport. 15th coastal engineering
851 conference, Honolulu, Hawaii, 1113-1133.

852 **Symons, W.O., Sumner, E.J, Talling, P.J., Cartigny, M.J.B.** and **Clare, M.A.** (2016) Large-scale
853 sediment waves and scours on the modern seafloor and their implications for the prevalence of
854 supercritical flow. *Mar. Geol.,* **371**, 130-148.

855 **Sylvester, S.** and **Covault, J.A.** (2016) Development of cutoff‐related knickpoints during early
856 evolution of submarine channels. *Geology.,* **44**, 835-838.

857 **Syvitski, J.P.M.** and **Farrow, G.E.** (1983) Structures and processes in bayhead deltas: Knight and Bute
858 Inlet, British Columbia. *Sediment. Geol.,* **36**, 217-244.

859 **Talling, P.J., Masson, D.G., Sumner, E.J.** and **Malgesini, G.** (2012) Subaqueous sediment density
860 flows: Depositional processes and deposit types. Sedimentology., 59, 1937-2003.

861 **Talling, P.J., Paull, C.K.** and **Piper, D.J.W.** (2013) How are subaqueous sediment density flows
862 triggered, what is their internal structure and how does it evolve? Direct observations from
863 monitoring of active flows. *Earth. Sci. Rev.,* **125**, 244-287.

864 **Talling, P.J., Allin, J., Armitage, D.A., Arnott, R.W.C., Cartigny, M.J.B., Clare, M.A… Xu, J.P.** (2015)
865 Key future directions for research on turbidity currents and their deposits. *J. Sediment. Res.,* **85**,
866 153-169.

867 **Torrence, C.** and **Compo, G.P.** (1998) A practical guide to wavelet analysis. *Bull. Am. Meteorol. Soc.,*
868 **79**, 61-78.

869 **Turmel, D., Locat, J.** and **Parker, G.** (2015) Morphological evolution of a well-constrained subaerial-
870 subaqueous source to sink system: Wabush Lake. *Sedimentology.,* **62**, 1636-1664.
871 **Van der Mark, C.F., Blom, A.** and **Hulscher, S.J.M.H.** (2008) Quantification of variability in bedform
872 geometry. *J. Geophys. Res. Earth Surface.,* **113**.
873 **Van Rijn, L.C.** (1984) Sediment transport, part III: bed forms and alluvial roughness. *J. Hydraul. Eng.,*
874 **110**, 1733-1754.
875 **Vendettuoli, D., Clare, M.A., Hughes Clarke, J.E., Vellinga, A., Hizzet, J., Hage, S., Cartigny, M.J.B.,**
876 **Talling, P.J., Waltham, D., Hubbard, S.M., Stacey, C.** and **Lintern, D.G.** (2019) Daily
877 bathymetric surveys document how stratigraphy is built and its extreme incompleteness in
878 submarine channels. *Earth. Planet. Sci. Lett.,* **515**, 231-247.
879 **Walker, R.G.** (1967) Turbidite sedimentary structures and their relationship to proximal and distal
880 depositional environments. *J. Sed. Petrol.,* **37**, 25-43.
881 **Wilbers, A.W.E.** and **Ten Brinke, W.B.M.** (2003) The response of subaqueous dunes to floods in sand
882 and gravel bed reaches of the Dutch Rhine. *Sedimentology*., **50**, 1013-1034.
883 **Xu, J.P., Sequeiros, O.E.** and **Noble ,M.A.** (2014) Sediment concentrations, flow conditions, and
884 downstream evolution of two turbidity currents, Monterey Canyon, USA. *Deep-Sea Research Part*
885 *I: Oceanographic Research Papers.,* **89**, 11–34.
886 **Zeng, J., Lowe, D. R., Prior, D. B., Wiseman, W. J.** and **Bornhold, B. D.** (1991) Flow properties of
887 turbidity currents in Bute Inlet, British Columbia. *Sedimentology.*, **38**, 975–996.
888 **Zhong, G.F., Cartigny, M.J.B., Kuang, Z.G.** and **Wang, L.L.** (2015) Cylic steps along the South
889 Taiwan Shoal and West Penghu submarine canyons on the northeastern continental slope of the
890 South China Sea. *GSA Bulletin.,* **127**, 804-824.
891
892

FIGURE CAPTIONS

Figure 1. (A) Submarine channel difference map of Bute Inlet between 2018 and 2008 highlighting channel dynamics. The positive values (blue) imply the deposition and negative values (red) imply erosion. Six acoustic Doppler current profilers (ADCP) were located on moorings placed from the proximal to the distal lobe of the channel. The Homathko and Southgate River deltas are the principal sources of sediment for the submarine channel. The study knickpoint (red dashed box) and a set of sediment cores are shown in Figs 7 and 9C. (B) Location of Bute Inlet in British Columbia, Canada.

Figure 2. (A) Schematic of turbidity-current frequency and runout from the six ADCP moorings between June and October 2016. The light-grey shade rectangle (upper right) denotes the period of time after failure of ADCP6 (Fig. 1) during the passage of a strong turbidity current. The dates of three major turbidity currents captured by ADCP3 are shown. (B) Velocity magnitude of a turbidity current event at ADCP3 on 20 June 2016.

Figure 3. (A) Longitudinal profile of the dominant submarine channel from the Homathko Delta to the distal lobe from the October 2016 bathymetric survey. Water depth varies from *ca* 58 m to *ca* 600 m. The red line (1.3 km) denotes the break of slope at the bottom of the Homathko Delta clinoform. The blue line (4 km) denotes the confluence of the Southgate Delta and the main channel. The black lines denote the locations of major knickpoints along the channel. (B) Channel longitudinal gradients. (C) Detrended channel profile showing bedform amplitude variation. Due to the vertical resolution of the survey, amplitudes smaller than 2 m and below *ca* 400 m depth between surveys should be considered with caution. (D) Wavelet power spectrum of the detrended channel profile. The colour scale shows spectral power of signal, which highlights the dominant frequency of variation (bedform wavelength) within the series. Red dashed boxes denote areas discussed in the *Crescentic bedform characteristics at the Homathko and Southgate deltas* section (labelled ‘a’) and *The influence of knickpoints on crescentic bedforms* section (labelled ‘b’), respectively.

Figure 4. (A) Geomorphology of the upper part of Bute Inlet submarine channel system. The blue and black lines represent the profiles of Homathko and Southgate deltas. The red dashed box represents

923 the subaqueous ridge (labelled ‘a’). (B) Longitudinal profiles of Homathko and Southgate deltas shown
924 in Fig. 4A. (C) Detailed bathymetric images of Homathko River Delta and (D) Southgate River Delta.
925
926 Figure 5. Analysis of crescentic bedform of the Homathko River Delta (A), (B) and (C) and Southgate
927 River Delta (D), (E) and (F). (A) and (D) water depth. (B) and (E) detrended profiles showing bedform
928 amplitudes with distance down delta clinoform; and (C) and (F) wavelet power spectrum. The colour
929 scale shows spectral power of signal, which highlights the dominant frequency of variation (bedform
930 wavelength) within the series.
931
932 Figure 6. Box plots of: (A) bedform height; (B) bedform wavelength; and (C) steepness (the ratio of
933 bedform height to wavelength) from Homathko 2016 survey data, Homathko 2018 survey data and
934 Southgate 2018 survey data. The tan and yellow colours denote the October 2016 and November 2018
935 Homathko River Delta surveys, respectively. The light-blue colour denotes the November 2018
936 Southgate River Delta survey.
937
938 Figure 7. Bathymetric images of the study knickpoint at June 2016 (A) and May 2018 (B). The results
939 show that the study knickpoint has migrated upstream *ca* 430 m during this period (Heijnen *et al.*, 2020).
940 The location of the study knickpoint is shown in Fig. 1A. (C) The difference map between May 2018 and
941 June 2016. The positive values (blue) imply the deposition and negative values (red) imply erosion.
942
943 Figure 8. Longitudinal profiles over the study knickpoint of June 2016 and May 2018. (A) and (D) Water
944 depth; (B) and (E) bedform amplitude; and (C) and (F) wavelet power spectrum. The red lines denote
945 the position of the knickpoint head. The blue lines denote the toe of the knickpoint. The black lines
946 denote the distalmost position of measured crescentic bedforms and the transition into a less variable
947 morphology.
948
949 Figure 9. (A) Longitudinal profiles of the study knickpoint in the June and October 2016 surveys. Blue
950 and red dots denote the sediment cores collected in June and October 2016, respectively. STN007
951 denotes the piston core and the rest of the cores refer to box cores. The potential hydraulic jump may
952 occur at *ca* 500 m. (B) Sedimentary logs from piston core and box cores located over the study

knickpoint. Note that the vertical scale of piston core STN007 is different from other box cores. (C) Plan view of the study knickpoint (as shown in Fig. 1A) and the locations of sediment cores. The locations of ADCP5 and ADCP4 are shown in the two sets of three black triangles each. The two triangles at both sides of each set, located on the channel bank and terrace, denote the two-point anchors and the central triangle denotes the ADCP location.

Figure 10 Conceptual model of different scales of bedforms and their distribution patterns over the knickpoint and resulting depositional signatures. The horizontal scale changes over the figure. The conceptual model is strongly vertically exaggerated.

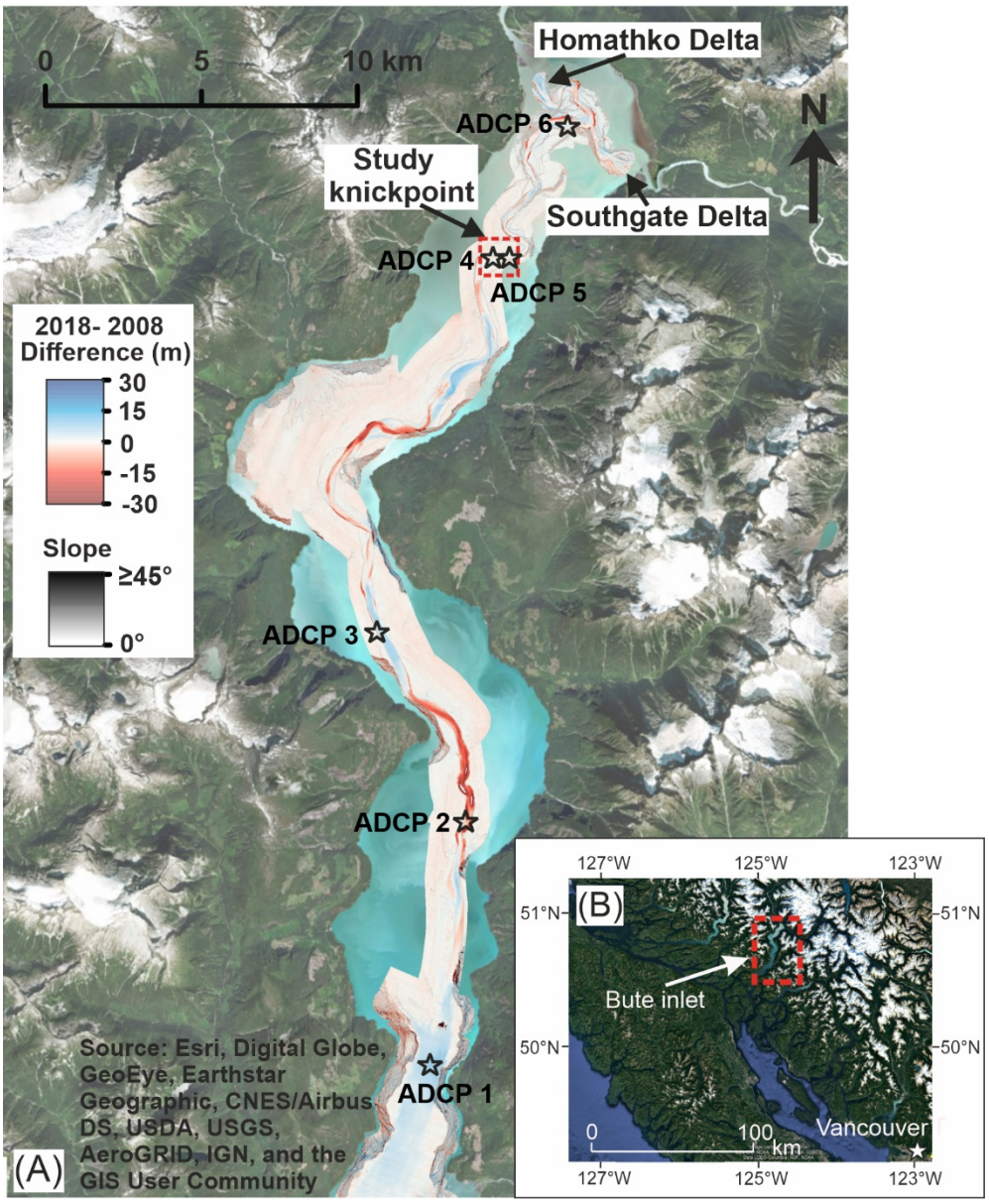

Figure 1. (A) Submarine channel difference map of Bute Inlet between 2018 and 2008 highlighting channel dynamics. The positive values (blue) imply the deposition and negative values (red) imply erosion. Six acoustic Doppler current profilers (ADCP) were located on moorings placed from the proximal to the distal lobe of the channel. The Homathko and Southgate River deltas are the principal sources of sediment for the submarine channel. The study knickpoint (red dashed box) and a set of sediment cores are shown in Figs 7 and 9C. (B) Location of Bute Inlet in British Columbia, Canada.

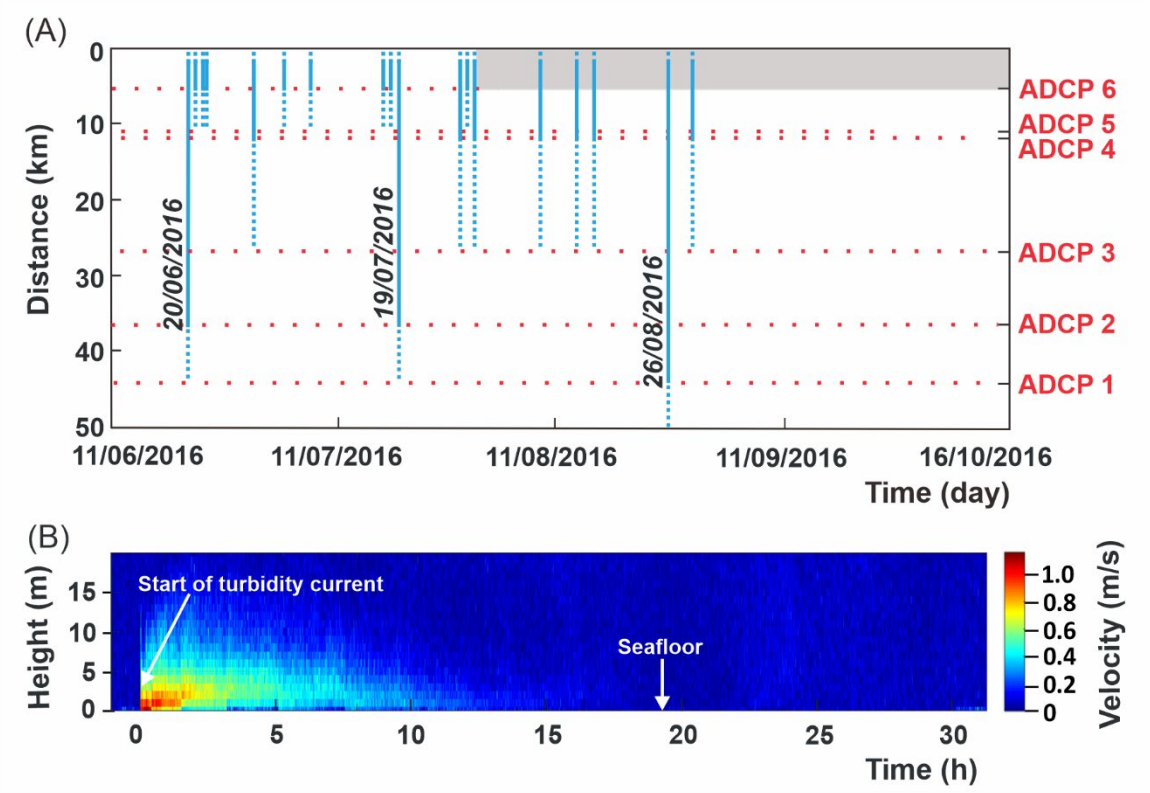

Figure 2. (A) Schematic of turbidity-current frequency and runout from the six ADCP moorings between June and October 2016. The light-grey shade rectangle (upper right) denotes the period of time after failure of ADCP6 (Fig. 1) during the passage of a strong turbidity current. The dates of three major turbidity currents captured by ADCP3 are shown. (B) Velocity magnitude of a turbidity current event at ADCP3 on 20 June 2016.

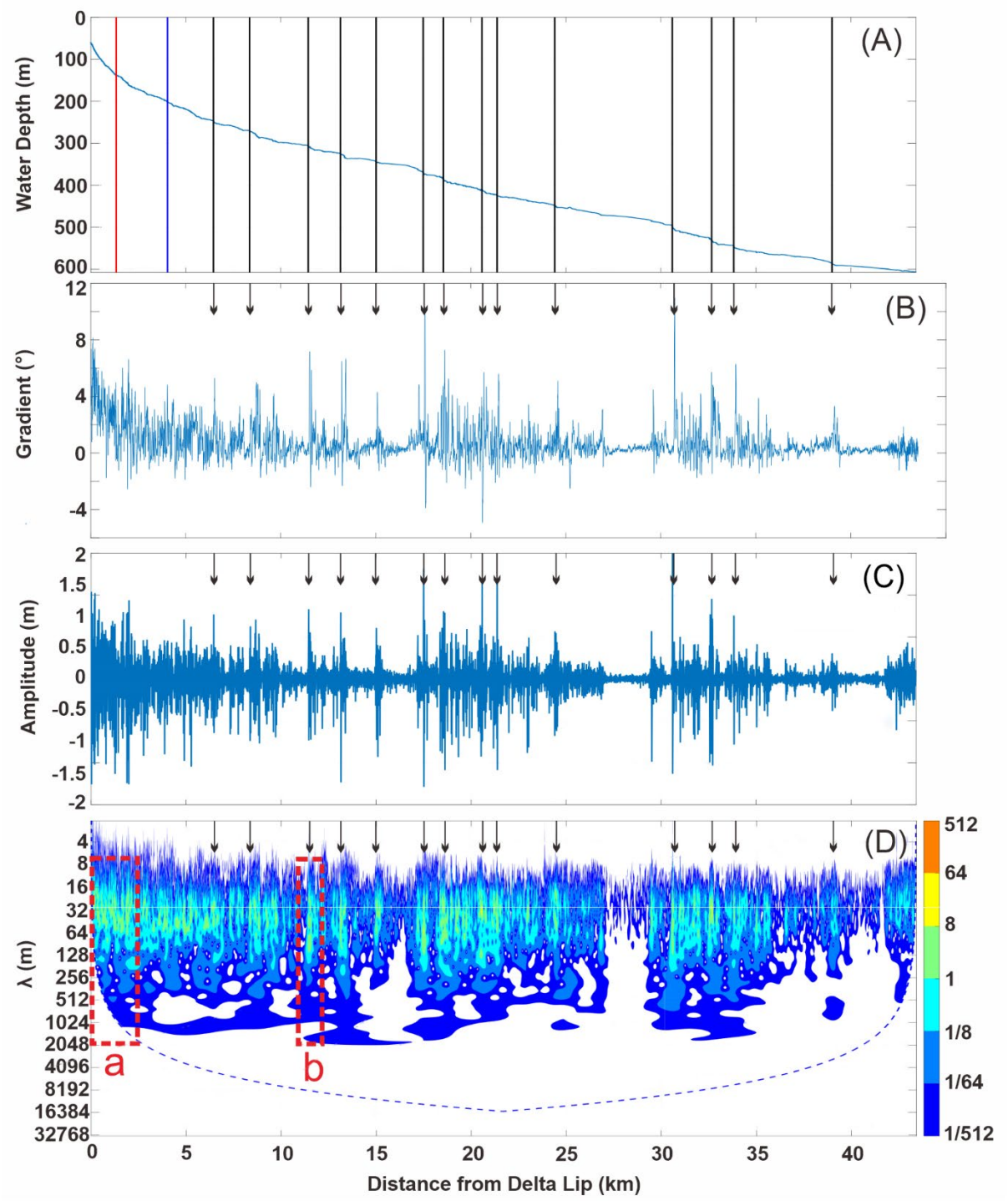

Figure 3. (A) Longitudinal profile of the dominant submarine channel from the Homathko Delta to the distal lobe from the October 2016 bathymetric survey. Water depth varies from *ca* 58 m to *ca* 600 m. The red line (1.3 km) denotes the break of slope at the bottom of the Homathko Delta clinoform. The blue line (4 km) denotes the confluence of the Southgate Delta and the main channel. The black lines denote the locations of major knickpoints along the channel. (B) Channel longitudinal gradients. (C) Detrended channel profile showing bedform amplitude variation. Due to the vertical resolution of the

survey, amplitudes smaller than 2 m and below *ca* 400 m depth between surveys should be considered with caution. (D) Wavelet power spectrum of the detrended channel profile. The colour scale shows spectral power of signal, which highlights the dominant frequency of variation (bedform wavelength) within the series. Red dashed boxes denote areas discussed in the *Crescentic bedform characteristics at the Homathko and Southgate deltas* section (labelled 'a') and *The influence of knickpoints on crescentic bedforms* section (labelled 'b'), respectively.

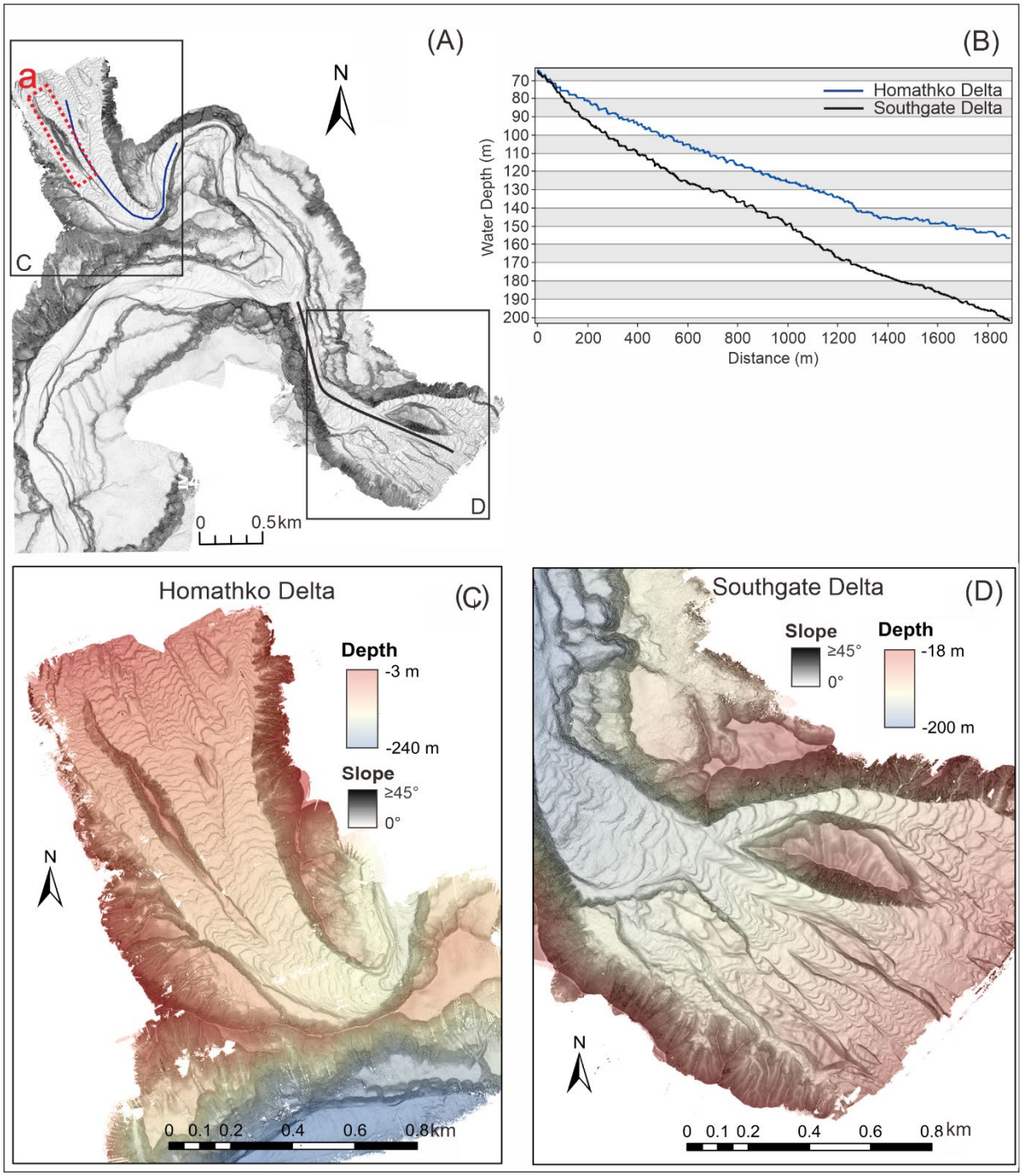

Figure 4. (A) Geomorphology of the upper part of Bute Inlet submarine channel system. The blue and black lines represent the profiles of Homathko and Southgate deltas. The red dashed box represents the subaqueous ridge (labelled ‘a’). (B) Longitudinal profiles of Homathko and Southgate deltas shown in Fig. 4A. (C) Detailed bathymetric images of Homathko River Delta and (D) Southgate River Delta.

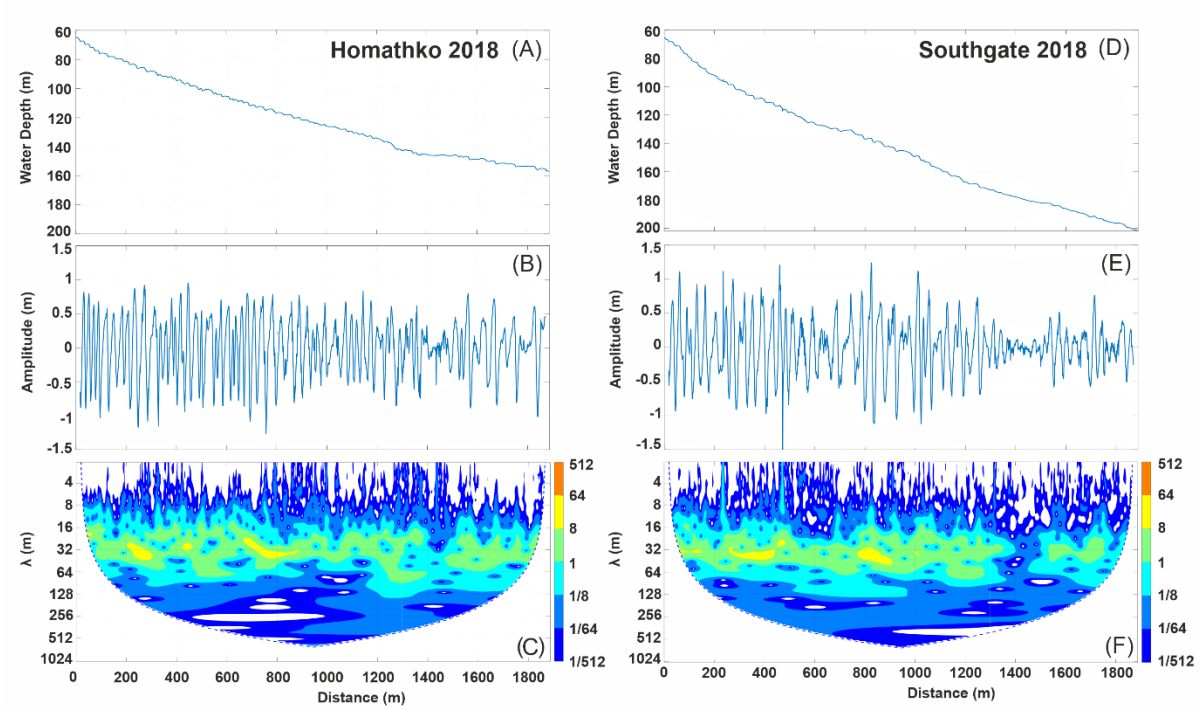

Figure 5. Analysis of crescentic bedform of the Homathko River Delta (A), (B) and (C) and Southgate River Delta (D), (E) and (F). (A) and (D) water depth. (B) and (E) detrended profiles showing bedform amplitudes with distance down delta clinoform; and (C) and (F) wavelet power spectrum. The colour scale shows spectral power of signal, which highlights the dominant frequency of variation (bedform wavelength) within the series.

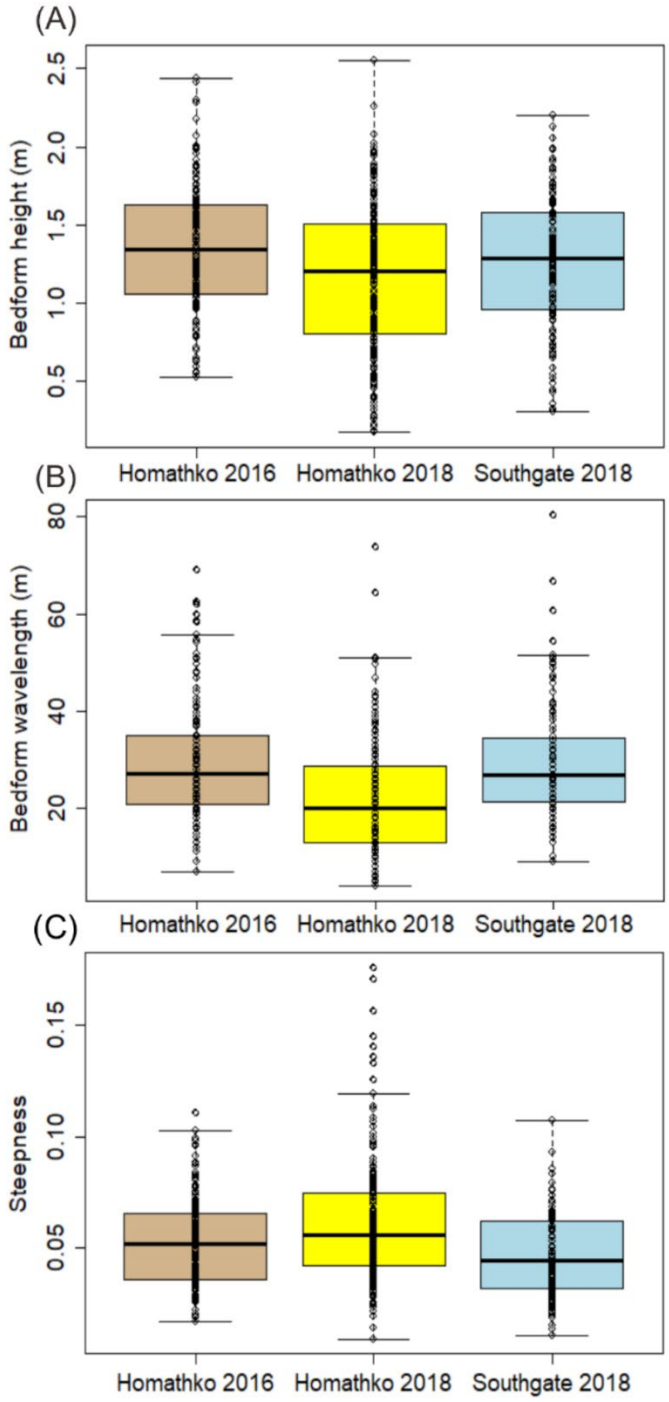

Figure 6. Box plots of: (A) bedform height; (B) bedform wavelength; and (C) steepness (the ratio of bedform height to wavelength) from Homathko 2016 survey data, Homathko 2018 survey data and Southgate 2018 survey data. The tan and yellow colours denote the October 2016 and November 2018 Homathko River Delta surveys, respectively. The light-blue colour denotes the November 2018 Southgate River Delta survey.

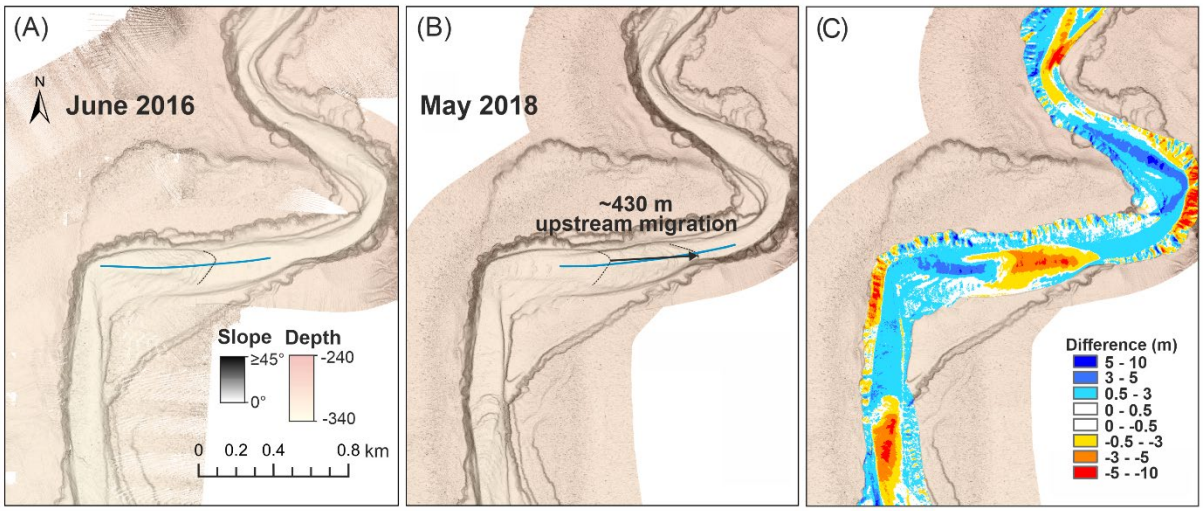

Figure 7. Bathymetric images of the study knickpoint at June 2016 (A) and May 2018 (B). The results show that the study knickpoint has migrated upstream *ca* 430 m during this period (Heijnen *et al.*, 2020). The location of the study knickpoint is shown in Fig. 1A. (C) The difference map between May 2018 and June 2016. The positive values (blue) imply the deposition and negative values (red) imply erosion.

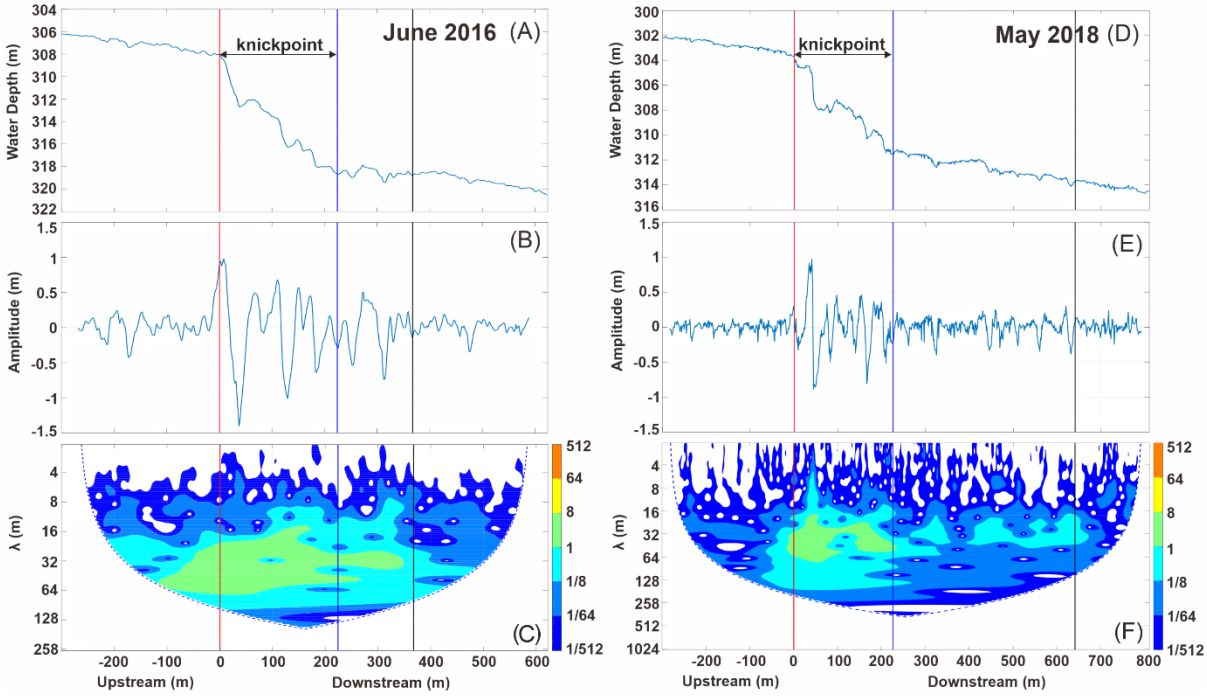

Figure 8. Longitudinal profiles over the study knickpoint of June 2016 and May 2018. (A) and (D) Water depth; (B) and (E) bedform amplitude; and (C) and (F) wavelet power spectrum. The red lines denote the position of the knickpoint head. The blue lines denote the toe of the knickpoint. The black lines denote the distalmost position of measured crescentic bedforms and the transition into a less variable morphology.

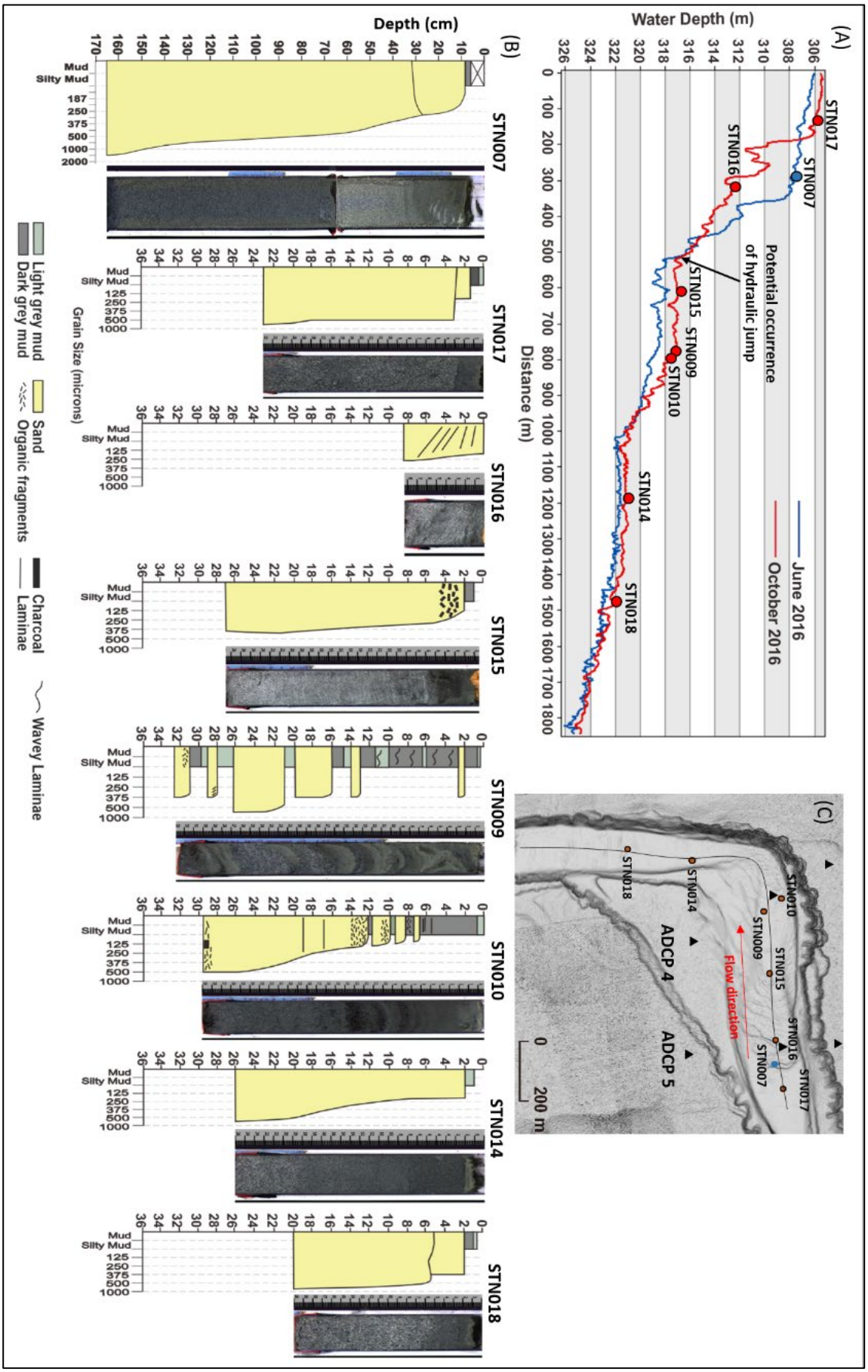
(A)
Water Depth (m)
Distance (m)
STN017
STN007
STN016
STN015
STN009
STN010
STN014
STN018
Potential occurrence of hydraulic jump
June 2016
October 2016
(B)
Depth (cm)
Grain Size (microns)
Mud
Silty Mud
125
250
375
500
1000
2000
STN007
STN017
STN016
STN015
STN009
STN010
STN014
STN018
Light grey mud
Dark grey mud
Sand
Organic fragments
Charcoal
Laminae
Wavey Laminae
(C)
STN017
STN016
STN007
STN010
STN015
STN009
STN014
STN018
ADCP 4
ADCP 5
Flow direction
0
200 m

1032

Figure 9. (A) Longitudinal profiles of the study knickpoint in the June and October 2016 surveys. Blue and red dots denote the sediment cores collected in June and October 2016, respectively. STN007 denotes the piston core and the rest of the cores refer to box cores. The potential hydraulic jump may occur at *ca* 500 m. (B) Sedimentary logs from piston core and box cores located over the study knickpoint. Note that the vertical scale of piston core STN007 is different from other box cores. (C) Plan view of the study knickpoint (as shown in Fig. 1A) and the locations of sediment cores. The locations of ADCP5 and ADCP4 are shown in the two sets of three black triangles each. The two triangles at both sides of each set, located on the channel bank and terrace, denote the two-point anchors and the central triangle denotes the ADCP location.

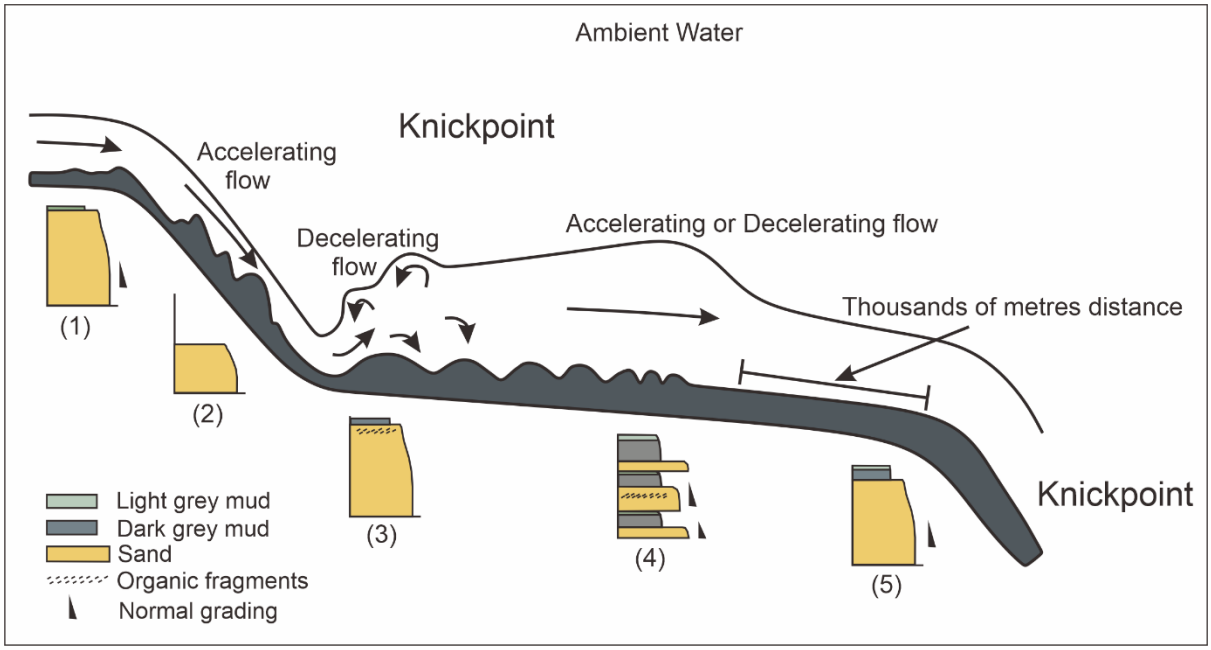

Figure 10 Conceptual model of different scales of bedforms and their distribution patterns over the knickpoint and resulting depositional signatures. The horizontal scale changes over the figure. The conceptual model is strongly vertically exaggerated.

Supplementary Table

CCGS Vector Survey		Resolution (m)	Coverage
March 2008		(5, 5)	Entire system
June 2016		(2, 2)	Entire system
October 2016		(1, 1)	Entire system
May 2018		(1, 1)	Entire system
November 2018		(1, 1)	Entire system
RV Strickland Survey			
October 2016		centimetric precision	Two deltas and upper channel
November 2018		centimetric precision	Two deltas and upper channel

Table 1. Overview of the date, resolution and coverage of CCGS *Vector* and RV *Strickland* surveys used in this study.

2016	Frequency (kHz)	Mean range to bed (m)
ADCP6	614.4	15
ADCP5	614.4	14
ADCP4	614.4	14
ADCP3	614.4	27
ADCP2	307.7	48
ADCP1	307.7	52

Table 2. The frequency and mean range to bed of six acoustic Doppler current profilers (ADCP).